Nanoscale Horizons

REVIEW

View Article Online
View Journal | View Issue

Cite this: *Nanoscale Horiz.*, 2025, **10**, 664

Biocomposites of 2D layered materials

Mert Vural and Melik C. Demirel *

Molecular composites, such as bone and nacre, are everywhere in nature and play crucial roles, ranging from self-defense to carbon sequestration. Extensive research has been conducted on constructing inorganic layered materials at an atomic level inspired by natural composites. These layered materials exfoliated to 2D crystals are an emerging family of nanomaterials with extraordinary properties. These biocomposites are great for modulating electron, photon, and phonon transport in nanoelectronics and photonic devices but are challenging to translate into bulk materials. Combining 2D crystals with biomolecules enables various 2D nanocomposites with novel characteristics. This review has provided an overview of the latest biocomposites, including their structure, composition, and characterization. Layered biocomposites have the potential to improve the performance of many devices. For example, biocomposites use macromolecules to control the organization of 2D crystals, allowing for new capabilities such as flexible electronics and energy storage. Other applications of 2D biocomposites include biomedical imaging, tissue engineering, chemical and biological sensing, gas and liquid filtration, and soft robotics. However, some fundamental questions need to be answered, such as self-assembly and kinetically limited states of organic–inorganic phases in soft matter physics.

Received 17th October 2024,
Accepted 6th January 2025

DOI: 10.1039/d4nh00530a

rsc.li/nanoscale-horizons

1. Introduction

The controlled assembly of 2D crystals with biomolecules is of particular interest as it allows for precise control over the physical properties of the resulting material. To achieve this, it is crucial to understand and control the molecular interactions between 2D crystals and complementary bio-systems. Using molecular biology tools, biomolecular-based materials that can initiate multiple physical or chemical interactions with 2D crystals are suitable for constructing functional bio-inorganic composites with programmable properties. This can lead to the development of several materials and devices for electronic, terahertz, and optics applications. Examples include metallic composites and organic conductor composites for electronic applications, insulating 2D graphene oxide for actuators and bolometers in terahertz applications, and protein-based waveguides, filters, and optical switches for optics applications. The foundation of next-generation, programmable, flexible, optically superior, energy-efficient, and mechanically solid materials and devices is established by 2D-layered materials.

In this review, we will thoroughly examine the interactions between biomolecules and 2D-layered composites. The paper will have three main sections: first, we will discuss the composition and structure of 2D biocomposites. Second, we will delve into various types of biomolecules used in 2D-layered composites, such as polysaccharides and polypeptides. Finally, we will summarize the unique properties that result from the interaction between these biomolecules and 2D-layered composites.

The exfoliation of layered materials into 2D crystals, starting with graphite,[1] introduced a new family of nanomaterials that exhibit extraordinary physical and chemical properties.[2,3] Beyond the individual qualities of these 2D materials, their proper combination with other materials projects a broad spectrum of composite materials with novel characteristics.[3–7] This prospect has developed significant research focus on 2D nanocomposites, in which 2D crystals, including graphene,[3,8,9] graphene oxide,[10,11] transition metal dichalcogenides (TMDCs),[12–15] 2D metal carbides, and nitrides (MXenes), single-element 2D-Xenes,[16,17] 2D dielectrics,[18–20] and black phosphorus[21,22] are coupled with organic and inorganic materials. These supplementary materials are synthesized,[23,24] assembled,[11,25–27] or processed[28,29] with 2D crystals to form functional composite materials. Inorganic materials are commonly synthesized or processed with 2D materials such as composites consisting of different 2D materials (heterostructures),[3,24,25] and nanomaterials (nanoparticles, nanotubes, and nanowires).[30,31] Inorganic 2D nanocomposites having a particular order in the nanoscale are promising for modulating electron,[31–33] photon,[34,35] and phonon[36] transport in nanoelectronics and photonic devices. However, it isn't easy to translate the precise structure of these nanocomposites into bulk materials and extend their utility

Center for Research on Advanced Fiber Technologies (CRAFT), Materials Research Institute and Huck Institute of Life Sciences, Pennsylvania State University, University Park, Pennsylvania 16802, USA. E-mail: melik@psu.edu

beyond laboratory-scale device applications.[37] Unlike inorganic 2D nanocomposites, composites composed of organic materials can be assembled and processed into bulk materials, hence finding a broader field of applications including flexible electronics,[38–40] and energy storage,[16,41,42] biomedical imaging,[43,44] chemical, and biological sensing.[45–48] However, organic 2D nanocomposites offer limited control over the organization of 2D crystals, mainly governed by the percolation of 2D crystals in an organic matrix.[26,28,29] The inferior control over the order of 2D crystals in organic 2D nanocomposites limits the utility of these composites in device applications. In recent years, research on organic 2D nanocomposites consisting of biomaterials has demonstrated that it is possible to control the organization of 2D crystals in these composites by exploiting the assembly mechanics of biomacromolecules, biopolymers, and bio-derived polymers.[10,26,40,49–51]

Biomolecular building blocks of 2D biocomposites commonly consist of polysaccharides (*e.g.*, cellulose, chitosan, alginates), polypeptides (*e.g.*, proteins), nucleic acids, and lipids. These biomacromolecules can form strong interactions with pristine or functionalized 2D crystals.[6] Hence, the initial studies concerning 2D biocomposites focus on exfoliating layered materials into 2D crystals with the help of biomacromolecules.[40,52–54] As the understanding of the interactions between 2D crystals and biomacromolecules built up, researchers started to develop bioinspired nacre-like materials that are much stronger and tougher than conventional composite materials.[4,49,55,56] The structural contribution of biomacromolecules to these biocomposite materials instigated more detailed research regarding the assembly mechanics of 2D crystals and biomacromolecules.[10,26,40,49] These studies unveiled a new set of materials in which biomacromolecules can modulate the physical aspects of composite materials beyond mechanical properties. The templating capability of biomacromolecules can help alter electronic,[26,51,57] thermal,[10,58–60] and optical[50,60,61] properties of composite materials *via* precise control over the structural organization of 2D crystals. The simplest biocomposites in which 2D crystals form a percolative network in biomacromolecule matrices can establish electronic materials that sustain a significant portion of their physical properties under mechanical deformation.[40,50,59,60,62] This feature is essential for materials that are employed in flexible electronics. Biomacromolecules can more profoundly influence the structural organization of 2D crystals in composites, where intercalating biomacromolecules can alter the interlayer spacing between 2D crystals with angstrom-level precision.[10,26,49] This templating capability can induce drastic changes in the isotropic and anisotropic electronic properties of biocomposites of 2D crystals. In addition, it is possible to generate electronic memory effects in these biocomposites.[26] Biomacromolecules can facilitate distinct interactions with chemical and biological materials. Once coupled to 2D crystals, these specific interactions can incite a change in their electronic properties.[26,40] This is the primary mechanism of detection for sensor devices based on 2D biocomposites.[40,45] Beyond electronic properties, biomacromolecules can also help regulate thermal transport in composites of 2D crystals.[10,58,60] Depending on the structural influence of the biomacromolecules on 2D crystals, 2D biocomposites can exhibit extraordinarily high and low (insulator) thermal conductivity.[58,60] Similar to electronic transport, the isotropy of thermal transport can be modulated by combining 2D crystals with proper biomacromolecules.[58,60] The structural impact of biomacromolecules on the organization of 2D crystals is significant in molding the light-matter interactions in 2D biocomposites.[40,50,60,61] Biomacromolecules can help 2D crystals alter their photoconductance through structural effects and specific interactions.[63] More importantly, biomacromolecules can induce a distinct separation between 2D crystals to drastically enhance their ability to trap electromagnetic waves, which results in 2D biocomposites with record-breaking electromagnetic shielding capabilities.[40,50] In addition to the structural order provided by biomacromolecules in the nanoscale, 2D crystals can also be combined with biomacromolecules to form microscale structures, which is more relevant for applications in energy storage.[16,64,65] The nanoscale order helps form channels for optimal ion transport, while the microscale order ensures the surface area needed to facilitate electrochemical reactions in energy storage systems.[64,65] Biomacromolecules also contribute to the structural integrity of these energy storage systems.[64,65] Besides energy storage, composites of biomacromolecules and 2D crystals show promise in transducing electrical, photonic, and thermal input into mechanical actuation.[10,53,66] 2D biocomposite actuators offer excellent alternative materials for applications in soft robotics, as they can be easily implemented into biological systems.[53,66] Other vital contributions of biomacromolecules to 2D composites are biocompatibility and the capability to interact with biological systems.[67–75] These features of 2D biocomposites are vitally crucial for biomedical applications such as tissue engineering,[67,70,71] drug delivery,[68,69,72,74,75] and antimicrobial materials.[73] The most recent field of application for 2D biocomposites is gas and liquid filtration, which utilizes the nacre-like structure of 2D biocomposites to form filtration membranes and specific interactions of biomacromolecules to trap targeted ions, molecules, and particles in these membranes.[76–80]

2. Structure and composition of 2D biocomposites

The introduction of 2D crystals with the demonstration of graphene presented a new set of materials with extraordinary physical and chemical properties.[1,81] After graphene, a plethora of 2D materials are extracted from layered materials by exfoliating single-few layered 2D crystals (graphene: 10 layers, MoS_2: 6 layers) or growing 2D crystals on specific substrates.[3] These 2D crystals exhibit extraordinary mechanical,[82] electronic,[2,3] thermal,[36,83,84] and optical[22,85–87] properties, significantly different from the bulk source material. However, these novel properties of 2D crystals diminish when the number of layers reaches a critical limit or individual 2D crystals interact.[3,81] These phenomena necessitate proper spacing between 2D crystals in composite systems to translate a significant portion of their unique aspects into composite materials. This engenders

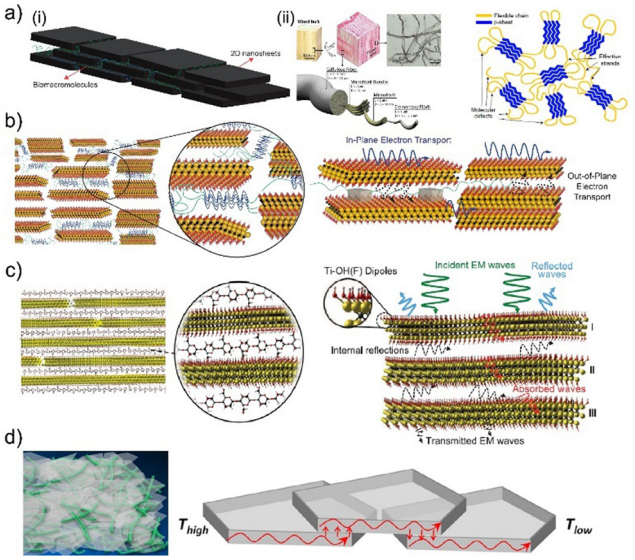

Fig. 1 (a) Schematic illustration of (i) self-assembly in biocomposites, (ii) hierarchical structure of cellulose from wood to nanofibrils, (iii) microstructure of polycrystalline proteins. Adapted with permission.[49,90,92] Copyright 2022, NAS, 2013, ACS, 2020, Springer Nature, respectively. (b) Schematics of the structure and electron transport in molecular composites consisting of synthetic repetitive proteins and conductive 2D crystals. Adapted with permission.[26] Copyright 2020, ACS. (c) Schematic of the structure and electromagnetic wave propagation in molecular composites consisting of naturally derived polysaccharides and conductive 2D crystals. Adapted with permission.[50] Copyright 2016, AAAS. (d) Schematics of the structure and thermal wave propagation in molecular composites consisting of cellulose and hexagonal boron nitride crystals. Adapted with permission.[93] Copyright 2014, ACS.

a bottleneck; as the volumetric fraction of 2D crystals decreases in composites, their contribution to physical properties drops exponentially, which is dictated by percolation theory.[29] Biomacromolecules can offer alternative assembly mechanics that differ from the composite matrix's random percolative distribution of 2D crystals.[26,88,89] These bio-macromolecular templates control the assembly of 2D crystals in biocomposites by facilitating specific interactions with 2D crystals and intercalating in between 2D crystals (Fig. 1(a)-(ii)).[10,26,40,49,51] Using the templating capability of natural and synthetic biomacromolecules, including polysaccharides[90] and polypeptides[91](Fig. 1(a)-(ii)), it is possible to reflect the unique properties of 2D crystals into bulk materials[10,26,49] and nurture new properties in 2D biocomposites.[10,26,49]

A recent study on 2D biocomposites composed of MXene nanosheets and recombinant proteins with repetitive amino acid sequences demonstrated that proteins consisting of 2D crystals could form a network between MXene nanosheets. This allowed MXene nanosheets to be processed using inkjet printing as responsive 2D biocomposites, which exhibit similar electronic properties as ordered MXene films.[40] A follow-up study has revealed that it is possible to systematically modify the interlayer spacing between MXene nanosheets using several repeat units in proteins as tuning parameters (Fig. 1(b)).[26] Systematic control over interlayer spacing between MXene nanosheets offers the ability to govern electron tunneling in these 2D biocomposites, which can be explained using a modified percolation theory.[26] This theory accurately predicts in-plane and out-of-plane electronic transport in 2D biocomposites until the interlayer spacing between 2D crystals becomes large enough to accommodate 2D crystals of synthetic proteins (Fig. 1(b)).[26] Once the number of tandem repeats in the protein sequence is sufficient to facilitate the formation of 2D protein crystals between MXene nanosheets, these 2D biocomposites demonstrate the electronic memory effect, which is absent in pristine MXene and protein films.[26]

Another 2D biocomposite of MXene nanosheets has utilized alginate to separate MXene nanosheets (Fig. 1(c)).[50] The primary role of alginate is to interconnect MXene nanosheets and improve mechanical integrity. However, the detailed investigation of the electromagnetic interference (EMI) shielding capabilities of these 2D biocomposites revealed another subtle but more important role of alginate: the separation it provides between MXene nanosheets (Fig. 1(c)).[50] This separation enhances the formation of internal reflections between MXene nanosheets, drastically improving the 2D biocomposite's EMI shielding efficiency. This structural contribution makes this material one of the best EMI shielding materials.[50]

Biocomposites of cellulose and hexagonal boron nitride (h-BN) nanosheets can be engineered to facilitate extraordinarily high[93] or low[94] thermal conductivity. Vacuum-assisted flocculation can help establish biocomposites of densely packed h-BN nanosheets in cellulose matrices (Fig. 1(d)).[93] These composites with nanoscale order have thermal conductivities higher than films of pristine h-BN nanosheets and other composites of h-BN nanosheets (Fig. 1(d)).[93,94] Cellulose acts as a binder in between h-BN nanosheets. Consequently, it enhances the interconnectivity of nanosheets and the contact area between nanosheets. This is the fundamental structural contribution of cellulose to the organization of h-BN nanosheets, which manifests itself as extraordinarily high thermal conductivity.[93]

In complementary to the structural templating capability of biomacromolecules, the ability to form specific interactions with 2D crystals is also critical to engineering functional materials from composites of biomaterials and 2D materials.[6] Biomacromolecules, including polysaccharides, polypeptides, nucleic acids, and lipids, can establish electrostatic, hydrophobic, π–π electron interactions, covalent and hydrogen bonding with pristine or modified 2D crystals.[6] These interactions can be strong enough to promote the exfoliation of 2D crystals from their bulk-layered source material (Fig. 2(a)-(i)–(iii)).[52,53,95–98] After exfoliation, biomacromolecules attached to the surface of 2D crystals form inclusion complexes. These inclusion complexes can help disperse these single—or few-layered 2D crystals in aqueous or non-aqueous solvents.[97] Orchestrating the intercalation of these complexes is the essence of controlling the structure and properties of resulting 2D biocomposites. In some instances, biomacromolecules interact more effectively with 2D crystals than the interactions they form with each other.[89,93,99] Biomacromolecules act as molecular separators/

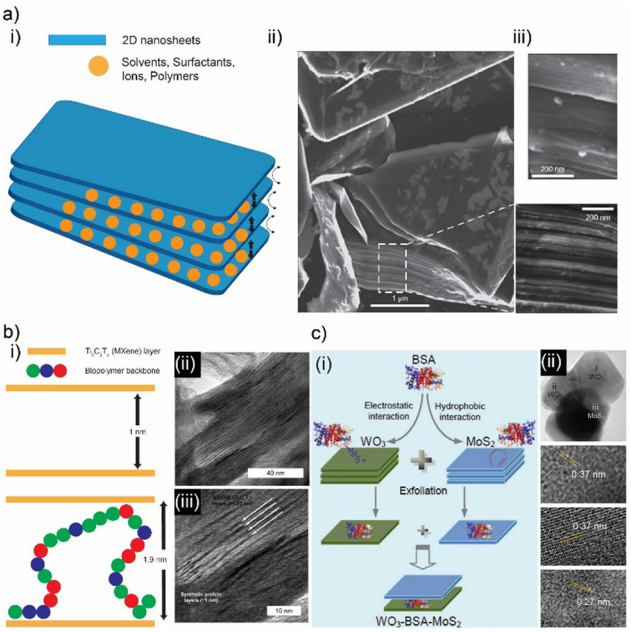

Fig. 2 (a) (i) Schematic illustration of intercalating molecules between 2D crystals. Scanning electron microscopy images of graphite nanosheets separated by phosphoric acid particles in perspective of graphite (ii) cross-section and (iii) plane. Adapted with permission.[98] Copyright 2014, Springer Nature. (b) (i) Schematic illustration of intercalating biopolymers between 2D crystals. (ii) Transmission electron microscopy images of biocomposites consisting of synthetic repetitive proteins intercalating in MXene nanocrystals. Adapted with permission.[26] Copyright 2020, ACS. (c) (i) Schematic illustration of alternating stacking of various transition dichalcogenide 2D crystals facilitated using bioderived polypeptides. (ii) Transmission electron microscopy images of stacked 2D crystals and spacer polypeptides. Adapted with permission.[27] Copyright 2017, Wiley-VCH.

intercalants in these composite materials (Fig. 2(b)).[89,93,99] In contrast to the simple structure of these biocomposites, macromolecules can construct more complex designs since they can establish different molecular interactions with each other and 2D crystals (Fig. 2(b)-(i)–(iii)).[10,26,27,49,51] Globular proteins (*e.g.*, bovine serum albumin, BSA) can facilitate hydrophobic interactions with MoS_2 and electrostatic interactions with WO_3 nanosheets.[27] It is possible to employ BSA to facilitate the formation of 2D heterostructures using solution-mediated self-assembly (Fig. 2(c)).[27] This is an excellent alternative for building 2D heterostructures since current methods require rigorous material growth and fabrication methodologies.[3] Beyond naturally derived proteins, recombinant proteins provide better control over possible interactions between proteins and 2D crystals.[6,10,26,49] Synthetic proteins can be designed to exhibit specific interactions with 2D crystals while they can still initiate multiple molecular interactions among themselves. This brings out another structural contribution: the ability to control the organization of 2D crystals with Angstrom-level precision and facilitate the formation of secondary structures between 2D crystals.[10,26,49] This generates unprecedented changes in the physical and chemical properties of the resulting 2D biocomposites.[10,26,49]

3. Family of 2D biocomposites

The advances in the spectrum of 2D materials have paved the way for new composite materials. In particular, recent research focus on composites consisting of 2D materials and macromolecules, biopolymers have led to a new set of biocomposites that can inherit the extraordinary properties of 2D materials and exhibit novel physicochemical properties originating from the diverse templating capabilities of biomaterials such as polysaccharides, polypeptides, and nucleic acids.[6,100] Polysaccharides are considered the most stable matrix material for composites compared to other macromolecules since they do not chemically degrade with moderate changes in temperature.[101] Besides stability, polysaccharides provide versatility in physical and chemical properties for their composites, which stem from their ability to form linear and branched biopolymers with various molecular weights.[101] Polypeptides offer more diverse structural templates for 2D materials than polysaccharides due to possible amino acid sequences of natural and recombinant proteins. The amino acid sequence defines protein folding, assembly, as well as secondary and tertiary structures.[100,102] Beyond individual structural characteristics of polypeptides, amino acid sequences can also be engineered to modulate the structural organization of 2D materials in a protein matrix that delineates biocomposites' exact physical and chemical properties.[10,26,49] Unlike polysaccharides that offer control over molecular weight and polymer structure, polypeptides grant additional parameters, including amino acid sequence and stereochemistry, to govern the design of biocomposites of 2D materials with Angstrom-level precision.[10,26,49]

3.1 Polysaccharide-based 2D biocomposites

Naturally abundant biomacromolecules and biopolymers of polysaccharides have recently manifested themselves as reliable alternatives to synthetic polymers as matrix material in composites. Common polysaccharide-based matrix materials include cellulose, chitosan, alginate, and pectin. These biopolymers acquired from natural resources form sustainable and biodegradable composites with 2D crystals. Biocomposites of polysaccharides and 2D crystals can exhibit extraordinary mechanical,[61,103] thermal,[58,93,104–106] electronic,[99,107,108] electromagnetic,[50,109,110] and electrochemical[111–113] properties.

3.1.1 Cellulose-based 2D biocomposites. Cellulose is the most abundant biopolymer, with annual production exceeding 700 billion tonnes globally.[101] Cellulose is commonly derived from plants.[101] However, it is possible to extract cellulose from bacteria with significantly different characteristics from plant-derived cellulose.[101] Cellulose is a homopolymer of glucose monomers connected *via* β (1, 4) glycosidic bonds. This long homopolymer can form intra- and inter-chain hydrogen bonding to generate a highly ordered molecular structure. The highly rated structure and the affinity to form hydrogen bonding are the main reasons behind cellulose's mechanically robust nature.[101,114] The hydrogen bonding groups in glucose monomers are also effective mediators for new chemical functional groups to expand the utility of cellulose.[114] Chemical

modification in cellulose results in new polymers like methylcellulose (MC), hydroxypropylmethylcellulose (HPMC), ethyl (hydroxyethyl)cellulose (EHEC), and cellulose nanocrystals oxidized *via* (2,2,6,6-tetramethylpiperidine-1-oxyl) (TEMPO), which happens to dissolve in water unlike pure cellulose and other derivatives (Cellulose acetate, CA), which swell in water.[114] Beyond its chemical adaptability and highly ordered molecular structure, cellulose also exhibits a fibrillar structure that can be replicated in multiple length scales, spanning from millimeters (wood chips) to nanometers (nanofabricated cellulose).[101,114] The structurally and chemically versatile nature of cellulose renders it a suitable matrix material for biocomposites of 2D materials, including graphene,[112,113] graphene oxide,[76,105] transition metal dichalcogenides (TMDCs),[115–117] MXenes,[61,118,119] hexagonal boron nitride (hBN),[93,94,106] black phosphorus.[120]

Graphene, particularly its water-processable derivatives like graphene oxide (GO) and reduced graphene oxide (rGO), generates functional biocomposites with various forms of cellulose. Functionalized cellulose crystals can interact with oxidized graphene crystals *via* hydrogen bonding, ionic[121] and hydrophilic interactions.[78,107] In the case of bacterial cellulose, oxidized graphene crystals can initiate covalent bonding with the help of mediator molecules.[122,123] Proteins and polysaccharides can also be used to connect graphene and its derivatives.[97,124] The structural organization of graphene crystals is defined by the initial form of cellulose (cellulose with microfibrils, nanofibrils, or bulk wood chips with cellular structure) and the density of the biocomposites they establish with cellulose. Cellulose is an excellent template material for constructing micro and nanoporous structures, which is essential to engineering low-density biocomposite materials.[101,114] Nanofibrils of cellulose can be effectively processed with aqueous solutions of GO to fabricate hydrogels. (Fig. 3(a)-(i)).[76] The trapped water in these hydrogels can be removed using freeze drying to form biocomposite foams consisting of a nano fibrillar network of cellulose and GO (Fig. 3(a)-(ii)).[76] GO is reduced once treated under excessive heat, and a conductive network of rGO is established (Fig. 3(a)-(ii)). Conductive nanofibrillar networks can sustain their structure through cyclic deformations, which also helps them maintain electrical conductivity during mechanical deformation (Fig. 3(a)-(iii)).[76] Besides electrical properties, nanocellulose-based foam structures can govern thermal transport in biocomposites (Fig. 3(b)-(i)).[105] Biocomposite foams assembled using freeze drying of nanocellulose/GO hydrogels can also be designed to have higher porosity (Fig. 3(b)-(ii) and (iii)).[105] In addition, implementing a heat gradient during hydrogel formation can help establish the formation of pores in a specific direction (Fig. 3(b)-(ii) and (iii)).[105] This makes these biocomposites exhibit enhanced mechanical strength and highly anisotropic thermal conductivity (radial: 15 mW mK^{-1}, axial: 170 mW mK^{-1}) (Fig. 3(b)-(iv)).[105] In contrast to microporous biocomposites, shrinking the pore size of biocomposites foams of cellulose and graphene derivatives to the nanoscale has a serious impact on energy storage devices relying on electrochemistry (Fig. 3(c)-(i) and (ii)).[113] The high surface area of the hierarchical nanostructure established from the hydrogels of nanofibrillated cellulose and reduced graphene oxide helps realize solid-state supercapacitors with excellent specific capacitance (207 F g^{-1})

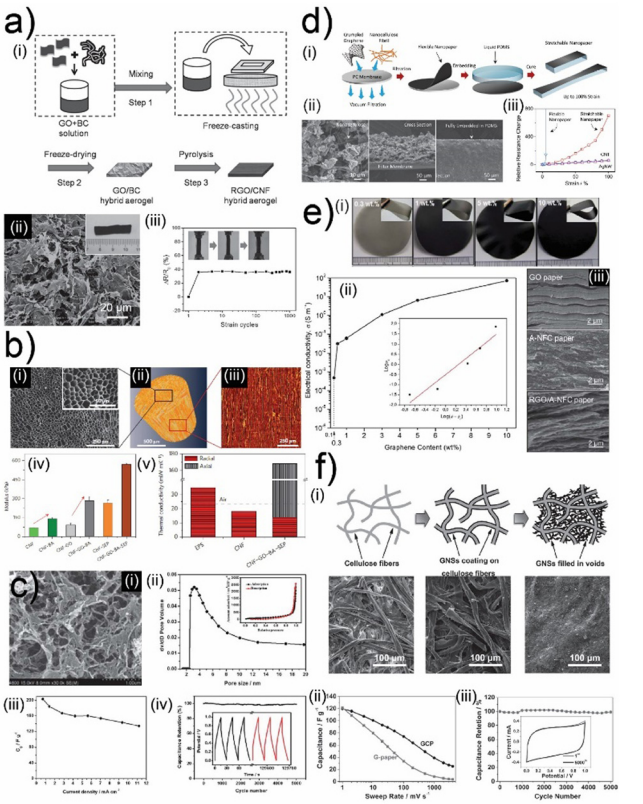

Fig. 3 (a) (i) Schematic illustration of fabrication for hydrogels and aerogels composed of graphene oxide (GO) cellulose. (ii) Scanning electron microscopy images of GO-cellulose aerogels. (iii) Normalized resistance of GO-cellulose aerogels during cyclic deformation. Adapted with permission.[76] Copyright 2017, Wiley-VCH. (b) (i) Scanning electron microscopy images of composites of nanofibrillated cellulose foams and GO crystals. (ii, iii) Reconstruction and original of X-ray microtomography images of foam composites of cellulose and GO crystals. (iv) Tensile modulus and (v) cellulose and GO crystal foam composites thermal conductivity. Adapted with permission.[105] Copyright 2015, Springer Nature. (c) (i) Scanning electron microscopy and (ii) pore volume images of highly porous GO-cellulose foams. Measurements of (iii) specific capacitance and (iv) capacitance retention during charge/discharge cycles. Adapted with permission.[113] Copyright 2013, RSC. (d) (i) Schematic illustration of fabrication for molecular composites of graphene crystals and fibrillar nanocellulose and their transfer on soft substrates. (ii) Scanning electron microscopy images of molecular composites transferred on soft substrates. (iii) Normalized resistance changes of molecular composites on soft substrates during continuous tensile deformation. Adapted with permission.[99] Copyright 2014, Wiley-VCH. (e) (i) Images of graphene and nanofibrillar cellulose molecular composites with different graphene filler concentrations. (ii) Conductivity of graphene and nanofibrillar cellulose molecular composites with different graphene concentrations. (iii) Scanning electron microscopy images of graphene, nanofibrillar cellulose nacres, and molecular composites of graphene and nanofibrillar cellulose. Adapted with permission.[125] Copyright 2011, RSC. (f) (i) Schematic illustration and SEM images of nanofibrillated cellulose, graphene-coated nanofibrillated cellulose, and composites of nanofibrillated cellulose and graphene crystals. Measurements of (ii) specific capacitance and (iii) capacitance retention during charge/discharge cycles for nanofibrillated cellulose and graphene crystal composites. Adapted with permission.[111] Copyright 2011, Wiley-VCH.

and cyclic stability (Fig. 3(c)-(iii) and (iv)).[113] Unlike low-density biocomposites, cellulose nanocrystals can govern the molecular assembly characteristics of graphene-based filler materials in compact biocomposites with higher density. Instead of building fibrillar cellulose templates that support graphene-based fillers, it is possible to utilize the specific interactions between cellulose and graphene derivatives to modulate the organization of graphene crystals in compact biocomposites.

The earlier studies investigating amine functionalized cellulose assembly mechanics with rGO suggest that the filler and the matrix material interact through hydrogen bonding (Fig. 3(d)-(i) and (ii)).[99] This strong interaction leads to the formation of biocomposites that exhibit good mechanical strength and electrical conductivity (Fig. 3(d)-(iii)).[99] This robust composite can be interfaced with elastomeric substrates to construct stretchable electrodes that can maintain a significant portion of their conductivity during deformation (Fig. 3(d)-(iii)).[99] Even though the fibrillar cellulose matrix did not impose a specific structural order, it acted as a bridge between conductive rGO nanoplatelets in molecular composites of cellulose and rGO (Fig. 3(e)-(i)–(iii)).[125] This structural influence helped these biocomposites to exhibit a low percolation threshold (Fig. 3(e)-(ii)).[125] Consequently, these biocomposites can reach high electrical conductivity values with moderate concentrations of rGO nanoplatelets (Fig. 3(e)-(ii)).[125] The porous template facilitated by the cellulose matrix is an excellent host for electrochemically active high-surface-area materials like graphene to establish high-performance electrochemical energy storage systems (Fig. 3(f)-(i)).[111] This cellulose-templated composite can reach promising gravimetric capacitance values of 120 F per gram of graphene (Fig. 3(f)-(ii)).[111] More importantly, this robust network structure enables the fabrication of robust supercapacitor systems that can operate consistently throughout many cycles (Fig. 3(f)-(iii)).[111]

Besides graphene, cellulose can also form conductive biocomposites with other 2D crystals such as layered MAX (M-early transition metals, A-Group A elements, and X–C, N, and additional functional surface groups) phases, *i.e.*, MXenes (Fig. 4(a)–(c)).[16,61] Vacuum-assisted self-assembly (VASA) of cellulose nanofibrils and MXene nanosheets through solution processing leads to a nacre-like structure (Fig. 4(a)-(i), (ii) and (b)-(i), (ii)). Biocomposites composed of larger nanofibrils exhibit lower electrical conductivity (8 S cm^{-1}) due to increased separation between MXene nanosheets (Fig. 4(a)-(iii)).[61] This structure also demonstrates extraordinary EMI shielding performance as the waves get trapped in between MXene nanosheets (Fig. 4(a)-(iv)).[61] Cellulose nanofibrils with smaller sizes lead to biocomposites with electrical conductivity values reaching 1000 S cm^{-1} (Fig. 4(b)-(iii)).[118] The nacre-like structure with smaller separation in between MXene nanosheets helps these biocomposites establish extraordinary mechanical properties and specific capacitance for energy storage applications (Fig. 4(b)-(iv)).[118] The extraordinary mechanical properties of these biocomposites originate from the hydrogen bonding formation between cellulose nanofibrils and MXene nanosheets

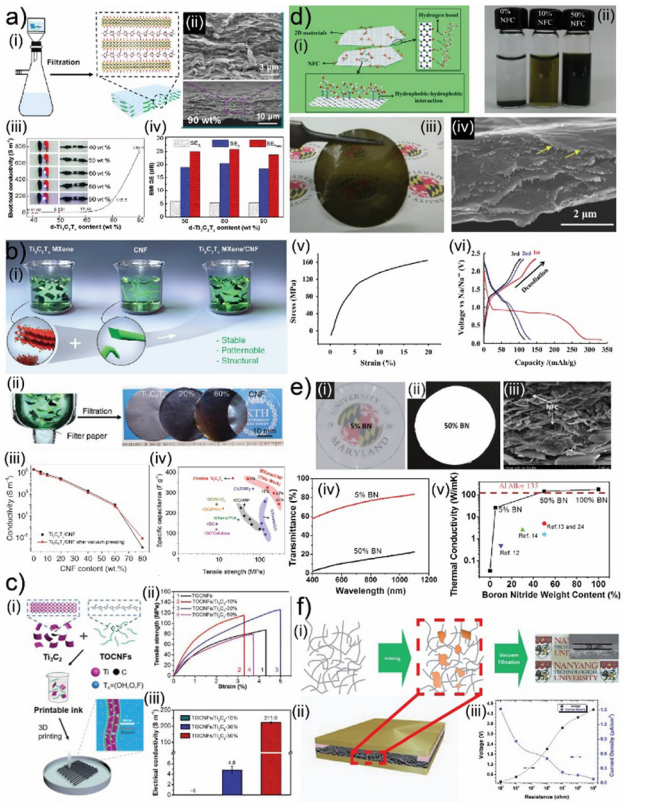

Fig. 4 (a) (i) Schematic illustration of self-assembly for molecular composites of cellulose and MXene crystals. (ii) Scanning electron microscopy images of molecular composites of cellulose and MXene crystals. (iii) Conductivity of molecular composites of cellulose and MXene crystals with different concentrations of MXene crystals. (iv) Electromagnetic interference (EMI) shielding properties of molecular composites of cellulose and MXene crystals with different concentrations of MXene crystals. Adapted with permission.[61] Copyright 2018, ACS. (b) (i) Schematic illustration and (ii) images of self-assembly for molecular composites of nanofibrillated cellulose and MXene crystals. (iii) The conductivity of molecular composites of nanofibrillated cellulose and MXene crystals with different concentrations of MXene crystals. (iv) Specific capacitance and tensile strength of molecular composites of nanofibrillated cellulose and MXene crystals. Adapted with permission.[127] Copyright 2019, Wiley-VCH. (c) (i) Schematic illustration of self-assembly for molecular composite inks of cellulose and MXene crystals. (ii) Tensile strength of composites printed from inks of cellulose and MXene crystals. (iii) The conductivity of composites printed from inks of cellulose and MXene crystals. Adapted with permission.[126] Copyright 2019, Wiley-VCH. (d) (i) Schematic illustration of self-assembly and exfoliation of 2D crystals through nanofibrillated cellulose. (ii) Images of 2D crystal solutions exfoliated using nanofibrillated cellulose. (iii) Images and (iv) scanning electron microscopy images of molecular composites of nanofibrillated cellulose and molybdenum disulfide crystals. (v) Stress/strain and (vi) charge/discharge profiles of molecular composites of nanofibrillated cellulose and molybdenum disulfide crystals. Adapted with permission.[128] Copyright 2015, Elsevier. (e) (i, ii) Images of hexagonal boron nitride and nanofibrillated cellulose molecular composites. (iii) Scanning electron microscopy image, (iv) optical transmission spectrum, and (v) thermal conductivity values of molecular composites of hexagonal boron nitride and nanofibrillated cellulose. Adapted with permission.[93] Copyright 2014, ACS. (f) Schematic illustration of (i) self-assembly for molecular composites of cellulose and black phosphorus crystals and (ii) energy generator device fabricated from these composites. (iii) Electronic properties of composites of cellulose and black phosphorus crystals. Adapted with permission.[120] Copyright 2017, Wiley-VCH.

(Fig. 4(a) and (b)).[61,118] This significant interaction is also utilized in the 3D printing of these biocomposites (Fig. 4(c)-(i)).[126] 3D-printed biocomposites demonstrate the percolative distribution of MXene nanosheets in a nano fibrillar cellulose matrix (Fig. 4(c)-(i)), which offers a more random distribution than self-assembled biocomposites.[126] This random distribution has minimal influence on mechanical properties (Fig. 4(c)-(ii)), but it leads to drastically low electrical conductivity (Fig. 4(c)-(iii)).[126]

Cellulose nanofibrils can establish hydrogen bonding and hydrophilic and hydrophobic interactions with other 2D crystals as well, including transition metal dichalcogenides (TMDCs), boron nitride (BN) nanosheets, and black phosphorus (bP) (Fig. 4(d)–(f)). These interactions benefit the delamination of these 2D crystals from their bulk counterparts (Fig. 4(d)-(i) and (ii)).[128] The exfoliated crystals can be assembled into free-standing films using VASA techniques (Fig. 4(d)-(iii) and (iv)).[128] Analogous to MXene-based biocomposites, TMDC-based biocomposites of nanofibrillated cellulose can also combine robust mechanical properties with good electrochemical properties (Fig. 4(d)-(v) and (vi)).[128] These properties help these biocomposites facilitate effective charging and discharging in sodium-ion batteries while operating as a working electrode (Fig. 4(d)-(vi)).[128] Cellulose nanofibrils can also help engineer thermal transport in biocomposites of 2D crystals (Fig. 4(e)).[93] Cellulose nanofibrils can assemble BN nanosheets into biocomposites with excellent thermal conductivity (Fig. 4(e)-(i)–(iii)).[93] Cellulose nanofibrils form bridges between BN nanosheets to keep them close and facilitate thermal transport between BN nanosheets (Fig. 4(e)-(iii)).[93] This structural integrity allows these biocomposites to exhibit thermal conductivities exceeding 100 W mK^{-1} and the ability to combine optical transparency with moderate thermal conductivity values for biocomposites with lower BN nanosheet concentration (Fig. 4(e)-(iv) and (v)).[93] In contrast to its structural contribution to graphene, MXene, TMDCs, and BN biocomposites, cellulose can act as a supporting and barrier matrix material for black phosphorus (Fig. 4(f)-(i)).[120] Black phosphorus nanocrystals can be trapped inside a nano fibrillar cellulose matrix to enhance the environmental stability of bP nanocrystals (Fig. 4(f)-(ii)).[120] This stable biocomposite can be used to fabricate triboelectric nanogenerator systems that utilize the extraordinary charging capability of bP nanocrystals without being concerned about the chemical degradation of bP (Fig. 4(f)-(ii) and (iii)).[120]

3.1.2 Chitosan and alginate based 2D biocomposites. Chitosan is another polysaccharide-based biopolymer extracted from the shells of shrimps and other crustaceans. Chitosan is a biopolymer composed of poly-D-glucosamine backbone terminated with acetylated end units (*N*-acetyl-D-glucosamine), capable of forming several interactions with 2D crystals, including hydrogen and covalent bonding.[129] Like cellulose, the chitosan backbone can initiate effective hydrogen bonding with 2D crystals like graphene oxide and MXene.[129,130] Chitosan can also form covalent bonds with these crystals through amine groups in its backbone, resulting in mechanically strong composites with nacre-like structures (Fig. 5(a)-(i)–(iii)).[129] Even though chitosan-based 2D biocomposites offer good mechanical properties, it is significantly more challenging to adjust the composition of these nacre-like composites using solution processing methods due to the low solubility of chitosan in aqueous solutions.[129] Hence, chitosan exhibits inferior templating capability compared to other polysaccharides, which is essential to govern the structure and physical properties of the resulting 2D biocomposites.[129] Nonetheless, the graphene oxide-based biocomposites of chitosan can demonstrate extraordinary mechanical properties like a combination of high mechanical strength (515 MPa) with high toughness (18 MJ m^{-3}) (Fig. 5(a)-(iv)).[129] This is particularly impressive, considering the volumetric concentration of chitosan is less than 5% in these 2D biocomposites, which indicates the significance of the interactions between chitosan and graphene oxide.[129] Besides, graphene oxide chitosan can form adequate hydrogen bonding with conductive MXene nanosheets and similarly form biocomposites with nacre-like structures (Fig. 5(b)-(i)–(iii)).[131] Various concentrations of chitosan can be intercalated between MXene nanosheets to construct composites with different electrical conductivity (Fig. 5(b)-(iv)).[131] The exponential scaling of the electrical conductivity with conductive filler (*e.g.*, MXene nanosheets) concentration indicates that chitosan is homogeneously and randomly distributed across the entire structure of these 2D biocomposites (Fig. 5(b)-(iv)).[131] A more significant impact of the intercalation of chitosan between MXene nanosheets is observed for the EMI shielding performance of these 2D biocomposites (Fig. 5(b)-(v)).[131] Although chitosan behaves like a regular matrix in these composites, intercalating chitosan molecules between MXene nanosheets establish a structure that helps trap electromagnetic waves in these composite materials (Fig. 5(b)-(v)).[131] This structure leads to 2D biocomposites that can reach EMI shielding effectiveness (SE) of 30 dB for composite films with a 30-micron thickness (thickness normalized effectiveness, SSE, of 9800 dB cm^{-1}) and 19 dB for composite films with a 13-micron thickness (SSE: 15150 dB cm^{-1}) (Fig. 5(b)-(v)).[131] Another bioderived polymer that can facilitate distinct interactions with 2D crystals is sodium alginate, which can intercalate between planar crystals (Fig. 5(c) and (d)).[50,132] In particular, graphene oxide can form hydrogen bonding networks with sodium alginate backbones and generate hierarchical assemblies (Fig. 5(c)-(i)). These assemblies produce nacre-like composite materials with extraordinary strength and toughness (Fig. 5(c)-(ii) and (iii)). In addition to graphene oxide nanocrystals, sodium alginate can form hydrogen bonding networks with MXene nanocrystals (Fig. 5(d)-(i)).[50] Sodium alginate intercalating between conductive MXene nanocrystals constructs a layered structure that significantly influences the electromagnetic blocking capabilities of MXenes (Fig. 5(d)-(i)–(iii)). Intrinsically, MXenes can absorb a significant portion of incoming electromagnetic radiation due to their conductive nature (Fig. 5(d)-(iv)).[40,50] However, this structural order also helps these composites trap electromagnetic radiation in these composites, which increases the number of absorbance events, hence significantly improving the electromagnetic

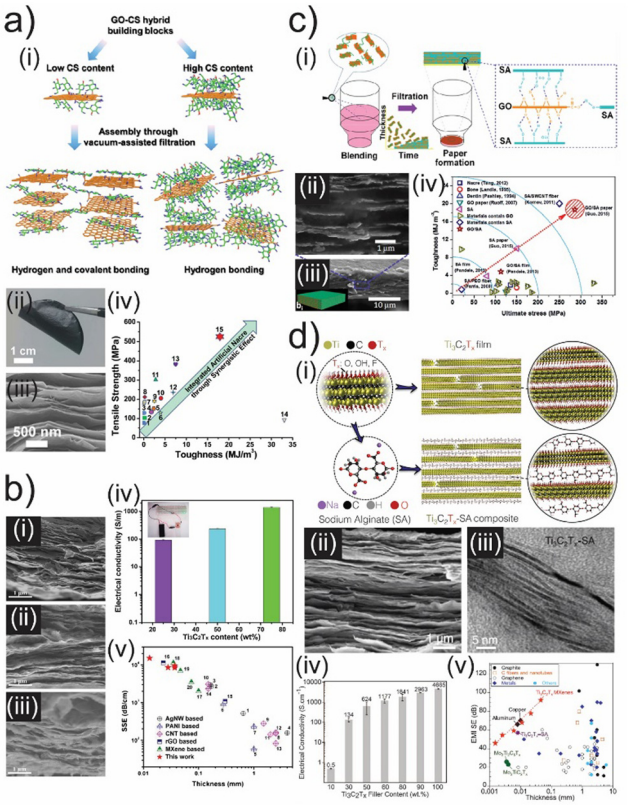

Fig. 5 (a) (i) Schematic illustration of self-assembly for nacre-like composites of chitosan and GO crystals. (ii) Images and (iii) scanning electron microscopy images of nacre-like composites of chitosan and GO crystals. (iv) Mechanical properties of nacre-like composites of chitosan and GO crystals. Adapted with permission.[133] Copyright 2015, ACS. (b) (i, ii, iii) Scanning electron microscopy images of nacre-like composites of chitosan and conductive MXene crystals. (iv) Conductivity and (v) EMI shielding properties of nacre-like composites of chitosan and conductive MXene crystals. Adapted with permission.[131] Copyright 2020, Elsevier. (c) (i) Schematic illustration of self-assembly for nacre-like composites of sodium alginate and GO crystals. (ii, iii) Scanning electron microscopy images of nacre-like composites of sodium alginate and GO crystals. (iv) Mechanical properties of nacre-like composites of sodium alginate and GO crystals. Adapted with permission.[132] Copyright 2015, ACS. (d) (i) Schematic illustration of self-assembly for nacre-like composites of sodium alginate and MXene crystals. (ii) Scanning electron microscopy and (iii) transmission electron microscopy images of nacre-like composites of sodium alginate and MXene crystals. (iv) Conductivity and (v) EMI shielding properties of nacre-like composites of sodium alginate and conductive MXene crystals. Adapted with permission.[50] Copyright 2016, AAAS.

radiation shielding capability of these materials (Fig. 5(d)-(ii)–(v)). This novel composite structure exhibits record-breaking electromagnetic interference (EMI) shielding capabilities as considerably thin material coatings (Fig. 5(d)-(v)).[50] This is only attainable due to structural assembly introduced into these composites through naturally derived biopolymers.[40,50]

3.2 Polypeptide-based 2D biocomposites

The success of polysaccharides as matrix materials in 2D composites has initiated research on composite materials based on other macromolecules, particularly polypeptides.[6,51,67,134] Polypeptides are produced from natural resources or biomanufacturing methods like fermentation.[102,135] Biomanufacturing enables large-scale production and, more importantly, engineering opportunities on the amino acid sequence of the polypeptides. The recent advances in synthetic biology can offer polypeptide designs with immense diversity, which renders polypeptides a better alternative for governing the structural organization of 2D crystal fillers in biocomposites.[6,135] The initial studies demonstrated that polypeptides acquired from natural resources could facilitate strong and specific interactions with various 2D materials, including graphene, GO, h-BN, MXenes, and TMDCs.[6] These studies have provided basic information concerning interactions between 2D crystals and polypeptides and paved the way for new studies based on engineered proteins.[6] Recent studies on composites of 2D crystals and recombinant proteins acquired from fermentation processes have revealed the true potential of polypeptides' templating capability in 2D biocomposites.[10,26,49] These works have demonstrated that it is possible to systematically alter composite materials' physical properties, including thermal, electronic, and mechanical properties, without being bound by the rules of percolation, which was unprecedented in composite materials.[10,26,49] Incorporating chitosan-based materials with 2D layered materials like molybdenum disulfide (MoS_2),[136] hexagonal boron nitride (h-BN),[137] and black phosphorus[138] indicates promising uses across different domains. Specifically, MoS2 holds promise for electronic devices,[136] h-BN acts as a catalyst,[137] and black phosphorus is valuable in electrochemistry.[138]

We recently studied atomically thin inorganic layers with tandem repeat proteins.[10,26,49] By controlling their molecular weight, we could fine-tune their mechanical properties, which exceeded those of state-of-the-art composites.[49] However, an existing theoretical model was unable to explain this phenomenon. Our findings suggest that the failure mechanism for composites depends more on interfacial rather than bulk properties.[49] Our inspiration for this study came from squid ring teeth, where recombinant proteins were found to adhere to inorganic sheets through secondary structures such as β-sheets and α-helices. This bonding mechanism resulted in high stretchability (59 ± 1% fracture strain) and toughness (54.8 ± 2 MJ m^{-3}).[49] We also discovered that the mechanical properties can be optimized by adjusting the protein molecular weight and tandem repetition. The exceptional mechanical responses we observed greatly exceeded the current state-of-the-art stretchability for layered composites by over a factor of three. This demonstrates the potential of engineering materials with reconfigurable physical properties.[49]

3.2.1 Naturally derived polypeptide-based 2D biocomposites. Proteins extracted from natural resources can be combined with 2D crystals to form functional biocomposites, as they can facilitate specific interactions with 2D crystal fillers similar to polysaccharide matrices in 2D biocomposites.[6] Naturally derived polypeptide materials like silk, gelatin,[67,70,71] silk,[51,54,134] and bovine serum albumin (BSA)[27,139] are matched with a variety of 2D crystals, including graphene, GO, h-BN, MXenes, and a large spectrum of TMDCs to form functional

2D biocomposites.[6] These polypeptide-based biomaterials extracted from natural resources interact with 2D crystals commonly through hydrogen bonding. Still, it is important to note that polypeptides are structurally and chemically more complex than polysaccharides and can form multiple interactions.[6,102] Depending on their amino acid sequence, hydrophilic, hydrophobic, and electrostatic interactions can be specific to 2D crystals and their chemically modified derivatives.[49,124] This is the most significant advantage of polypeptide-based matrix materials compared to polysaccharide-based matrix materials in 2D biocomposites.

Naturally derived polypeptides have demonstrated intriguing assembly characteristics when matched with graphene and its derivatives,[45,67,71,140] which incited many recent studies on polypeptide-based 2D biocomposites.[26,49,51] In particular, silk fibroin can form various structures, from nano micelles to single molecule protofibrils on the surface of graphene derivatives, depending on the fibroin concentration, pH, humidity, and other physical conditions.[45,67,71,140] BSA is another naturally derived polypeptide that can facilitate strong interactions with graphene,[139] which is also commonly employed to exfoliate layered bulk materials to generate 2D crystals.[52,141] These fundamental studies have helped develop an understanding of the physical properties of biocomposites fabricated from 2D crystals and naturally derived polypeptides. Silk and amyloid fibrils have formed functional composite materials with graphene derivatives (Fig. 6(a) and (b)).[45,134] Silk has proven to be an effective matrix material for constructing mechanically tough and strong 2D biocomposites (Fig. 6(a)-(i) and (ii)).[134] On the other hand, amyloid fibrils facilitated the specific assembly of 2D crystals, which resulted in enhanced interconnectivity of conductive graphene oxide fillers and, consequently, higher electrical conductivity (Fig. 6(b)-(i) and (ii)).[45] The assembly kinetics of amyloid fibrils and graphene oxide nanosheets have also led to anisotropic mechanical properties (Fig. 6(b)-(iii)).[45] The interactions between graphene derivatives are also used to construct hydrogel structures, wherein filler materials are employed to cross-link naturally derived gelatin matrix.[67,71] Gelatin can also be processed with graphene derivatives and h-BN nanosheets to form nacre-like structures, which can be used to construct mechanically robust biomaterials.[70] Beyond graphene derivatives, other conductive 2D filler materials like MXenes can create specific assemblies with silk fibroin (Fig. 6(c)). However, unlike amyloid fibrils, these assemblies did not incite controllable changes in the electrical properties of the resultant 2D biocomposite.[51] Silk fibroin instead acts as a mechanical support and protective enclosure against oxidation of MXenes (Fig. 6(c)), which tends to degrade their electronic and optical properties.[51]

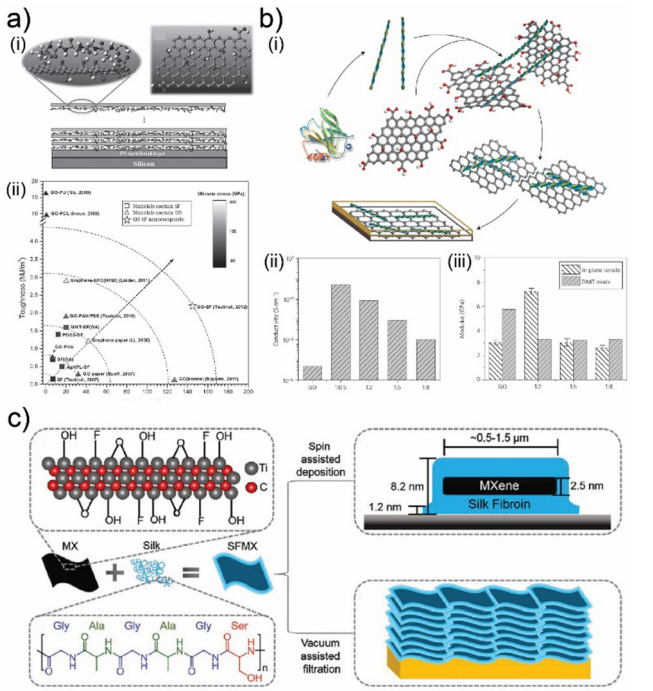

Fig. 6 (a) (i) Schematic illustration of self-assembly for nacre-like composites of silk fibroin and GO crystals. (ii) Mechanical properties of nacre-like composites of nacre-like composites of silk fibroin and GO crystals. Adapted with permission.[134] Copyright 2013, Wiley-VCH. (b) (i) Schematic illustration of self-assembly for nacre-like composites of amyloid fibrils and GO crystals. (ii) Conductivity of nacre-like composites of amyloid fibrils and GO crystals. (iii) Tensile modulus of nacre-like composites of amyloid fibrils and GO crystals. Adapted with permission.[45] Copyright 2015, Springer Nature. (c) Schematic illustration of self-assembly for nacre-like composites of silk and MXene crystals. Adapted with permission.[51] Copyright 2020, Wiley-VCH.

3.2.2 Recombinant polypeptide-based 2D biocomposites. The good physical properties observed from 2D biocomposites consisting of naturally derived polypeptide matrix materials have encouraged researchers to investigate the performance of recombinant polypeptides as matrix materials in 2D biocomposites. Recombinant polypeptides can be more versatile molecular templates for 2D crystal fillers, considering the possibility of modifying the amino acid sequences that govern the polypeptide matrix material's inter and intramolecular interactions.[6,10,26,49,124] The initial studies focusing on recombinant polypeptide assemblies on individual 2D crystals have demonstrated that introducing specific amino acid sequences responsible for binding to 2D crystals manifests the assembly mechanics of polypeptides on 2D crystals.[10,88,124,142] Depending on polypeptide sequence and 2D crystal surface chemistry, proteins can fold into nanowires to globular conformations at the surface of the 2D crystals (Fig. 7(a)).[88,142] These earlier studies have also unveiled that it is possible to modify hydrophilic and hydrophobic interactions formed by recombinant polypeptides through modifications in amino acid sequences or engineered amino acid sequences that can undergo phase transitions when probed with heat or light (Fig. 7(b) and (c)).[97,143] These phase transitions can be employed to adjust the arrangement of graphene crystals in 2D biocomposites, which inherently corresponds to a mechanical actuation (Fig. 7(d)).[144] Different from large-scale organizational changes in the structure of 2D biocomposites, the amino acid sequence of polypeptides can also be employed to control the assembly of 2D crystals in 2D biocomposites with angstrom-level precision.[10,26,49] In the case of GO crystals, systematic control over interlayer distances between GO crystals

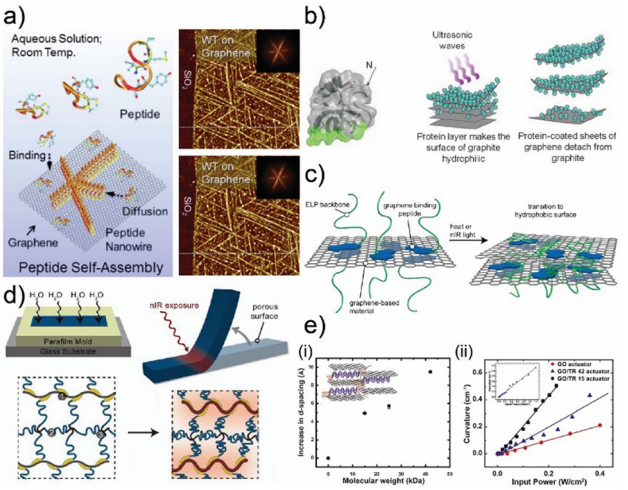

Fig. 7 (a) Schematic illustration and atomic force microscopy images of self-assembly of recombinant proteins and GO crystals. Adapted with permission.[142] Copyright 2016, Springer Nature. (b) Schematic illustration of recombinant proteins and their assembly mechanics on graphene crystals. Adapted with permission.[97] Copyright 2010, Wiley-VCH. (c) Schematic illustration of synthetic proteins derived from elastin-like proteins and their response to physical probing. Adapted with permission.[143] Copyright 2014, ACS. (d) Schematic illustration of graphene–gelatin composites and their response to infrared radiation. Adapted with permission.[144] Copyright 2013, ACS. (e) (i) The interlayer distance between GO crystals as a function of the molecular weight of recombinant repetitive proteins. (ii) The influence of structural order introduced by synthetic proteins on the actuation performance of their composites with GO crystals. Adapted with permission.[10] Copyright 2017, Elsevier.

helps govern thermal transport in 2D biocomposites (Fig. 7(e)-(i)).[10] By simply adjusting the number of tandem repeat units in the amino acid sequence, it is possible to acquire 2D biocomposites with significantly different mechanical properties and thermal actuation performance (Fig. 7(e)-(ii)).[10] Shorter amino acid sequences produce actuation materials with better energy efficiency and low elasticity. Longer amino acid sequences offer actuation materials with low energy efficiency and better elasticity (Fig. 7(e)-(ii)).[10] This templating capability of recombinant proteins can also be used to associate other functional nanomaterials with graphene and its derivatives.[64,145] Altering the amino acid sequence of binding proteins is introduced into graphene nanoparticle systems to help form conductive pathways on graphene crystals and engender novel composite materials for energy storage.[64] Besides assembling graphene crystals, the amino acid sequence of recombinant proteins can be modified to construct nanowires from graphene crystals, a promising building block for graphene-based hydrogel structures.[145]

The recombinant polypeptides can also form functional assemblies with a new family of 2D crystals like MXenes.[16] MXene nanocrystals can interact with naturally derived and synthetic polypeptides based on silk and squid ring teeth, commonly through hydrogen bonding and charge interactions.[10,26,49,51,146] These interactions can be programmed to define the overall organization of graphene oxide and MXene nanocrystals.[10,26] In a more complex system consisting of more than 2D crystal, synthetic proteins elect to organize a single 2D crystal while the secondary 2D crystal acts as a percolative filler material (Fig. 8(a)-(i)).[49] This is reflected in the assembly characteristics of the 2D crystals that are systematically separated by synthetic proteins (Fig. 8(a)-(ii)).[49] It is possible to explain this assembly characteristic by implementing interfacial interactions between 2D crystals and repetitive proteins.[49]

This physical model reveals that the structural organization of these two distinct 2D crystals orchestrated by synthetic proteins and interfacial interactions can engender structural material systems that exhibit extraordinary toughness (Fig. 8(b)-(i)).[49] Unlike existing structural materials engineered using synthetic chemistry, these structural materials programmed using synthetic biology employ enhancements in the extent of deformation instead of improving material strength (Fig. 8(b)-(ii)).[49] This unorthodox approach helps these novel materials match and overcome the toughness of the strongest composites based on 2D crystals (Fig. 8(b)-(ii)).[49] Another important aspect of this approach is the ability to modify this enhancement systematically using the amino acid sequence of these repetitive proteins.[49] In a more straightforward material system composed of MXene nanocrystals and these repetitive proteins, the organization of conductive MXene crystals is altered with precision to govern electronic transport in a composite material (Fig. 8(c)-(i)).[26] Besides percolative distribution simply relying on the volumetric concentration of the conductive filler material, synthetic repetitive proteins offer a more refined control over the tunneling distance between MXene nanocrystals among a bulk freestanding composite (Fig. 8(c)-(ii)).[26] The influence of this structural control over tunneling distance can be easily modeled and confirmed using experimental conductivity measurements, which confirms the overall organization of MXene crystals is indeed governed by self-assembly kinetics defined by the amino acid sequence of these repetitive proteins (Fig. 8(c)-(ii)).[26] This model is also indicative of a topological order in these conductive composite materials, which is documented by the distinct difference between in-plane and out-of-plane electron transport among these bulk composites (Fig. 8(c)-(ii) and d-(i)). The physical model and experimental investigation of out-of-plane electronic conductivity indicated a critical dimension for a transition from electron-dominated transport to ion-dominated transport in between MXene nanocrystals (Fig. 8(d)-(ii)).[26] Once the separation between MXene nanocrystals becomes large enough to accommodate the formation of beta-sheet crystals, these composites exhibit an electronic memory behavior (Fig. 8(d)-(ii)).[26] Globular and structural proteins are known to exhibit memory effects in more delicate device geometries based on lithographic fabrication methods. However, this is one of the first demonstrations of memristive behavior in bulk materials, particularly based on biocomposites.[57,147,148]

3.3 Nucleic acid-based 2D biocomposites

Nucleic acids, such as DNA and RNA, have been increasingly explored as functional components in developing innovative 2D layered composites.[6,100] These composites, often consisting of

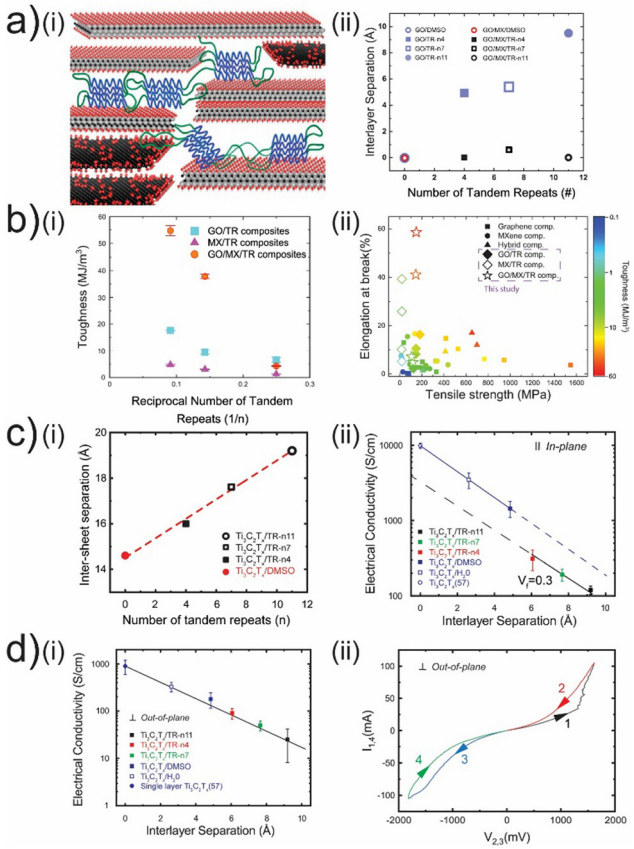

Fig. 8 (a) (i) Schematic illustration of self-assembly for molecular composites of synthetic repetitive proteins and 2D crystals (GO and MXene). (ii) The interlayer distance between 2D crystals as a function of the number of repeat units of repetitive proteins in these molecular composites. (b) (i) The influence of the number of repeat units on the mechanical toughness of these molecular composites. (ii) The landscape of mechanical properties of existing 2D composites and their comparison with these molecular composites. Adapted with permission.[49] Copyright 2022, NAS. (c) (i) The interlayer distance between MXene crystals as a function of the number of repeat units of repetitive proteins for molecular composites of repetitive proteins and MXene crystals. (ii) The experimental and theoretical in-plane conductivity of these molecular composites as a function of the interlayer separation between MXene crystals. (d) (i) The experimental and theoretical out-of-plane conductivity of these molecular composites as a function of the interlayer separation between MXene crystals. (ii) *I*/*V* curve of molecular composites composed of synthetic repetitive proteins with 11 repeat units exhibiting resistive memory effect. Adapted with permission.[26] Copyright 2020, ACS.

graphene or graphene oxide, offer exceptional mechanical, thermal, and electrical properties have been obtained. By integrating nucleic acids into these 2D layered structures, hybrid materials with enhanced functionality, such as biosensing, drug delivery, and tissue engineering capabilities. For example, it has been shown that the construction of nucleic acids on the surface of graphene has a strong sensitivity to metal ions,[149] and can also enhance its electrochemical performance.[150]

3.4 Summary of materials properties of 2D biocomposites

To summarize the available 2D biocomposites, we created a table outlining composite materials consisting of different 2D crystals and biopolymers. These materials can form a hierarchical order that translates to novel physical properties, as shown in Table 1. In the current state of composite theory, 2D biocomposites predominantly rely on the filler fraction as a primary parameter to modify the physical characteristics of the resultant composites. The potential of biopolymers is reflected in their ability to attain a wide range of properties, which can be adjusted across multiple orders of magnitude. This extensive range is difficult to achieve using filler fraction alone, as it is limited by the rules of percolation. Therefore, biopolymer assembly characteristics, including hydrogen bonding networks, charge, and hydrophobic interactions, are utilized to create 2D biocomposites with novel material properties. In recent years, there has been a push to separate the structural influence from the filler fraction by introducing a secondary parameter that defines this influence. To achieve this, researchers have developed bioengineered proteins with a distinct number of identical repetition units among their amino acid sequences.[151] The number of repetition units helps define the interlayer separation between 2D crystals with Angstrom-level precision, hence introducing a definite model for electrical conductivity,[26] mechanical deformation,[49] and electromagnetic shielding.[40] This secondary parameter has extended the range of physical aspects to be engineered across three orders of magnitude and even enabled the conversion of physical behavior like switching from conductive to memristive (*i.e.*, observed in thin dielectrics) state.[26] Other researchers follow these works, employing similar block copolymer-like protein sequences, such as silk, to establish functional 2D biocomposites.[51] We believe the advances in synthetic biology tools will drive this approach further as new protein designs become available to match the surface chemistry of an ever-growing family of 2D crystals. This way, the fundamentals of composite research will be redefined as novel matrix materials developed by protein researchers will introduce a new set of parameters for engineering composite materials.

4. Conclusions and future prospects of 2D biocomposites

The molecular architecture of layered composites was inspired by exoskeletons and endoskeletons, which rely heavily on polypeptides and polysaccharides, such as collagen or chitin. The evolutionary paths of exoskeletons and endoskeletons are intertwined. Early life forms probably lacked either type of structure, but support systems emerged as creatures became more complex. They became internalized and bony, providing strong support for muscles and organs. Meanwhile, exoskeletons took various forms like shells or scales, offering protection but limiting growth potential. The future of layered composites will go beyond imitating nature, as sustainable materials and high-performance biocomposites make them more competitive with established materials.

Layered composites hold great promise for the future, as they allow the properties of different materials to be combined. An important area for development will be the customization of

Table 1 Composite materials consisting of different 2D crystals and biopolymers

	Biopolymer	2D crystal	Physical properties	Control parameter	Range
Ref. 103	Nanocellulose	Graphene	Tensile strength Tensile modulus Elongation at break Toughness	Filler fraction	170–351 MPa 8–16.9 MPa 9–12% 11–22 MJ m^{-3}
Ref. 61	Nanocellulose	MXene	Tensile strength Tensile modulus Elongation at break Toughness Electrical conductivity EMI shielding	Filler fraction	42–135.4 MPa 1–3.8 GPa 3–16.7% 1.2–15 MJ m^{-3} 0.62–739 S cm^{-1} 1200–2647 dB cm^2 g^{-1}
Ref. 93	Nanocellulose	Hexagonal boron nitride	Thermal conductivity	Filler fraction	0.04–145 W m^{-1} K^{-1}
Ref. 106	Nanocellulose	Hexagonal boron nitride	Thermal conductivity	Filler fraction	0.184–3.13 W m^{-1} K^{-1}
Ref. 105	Nanocellulose	Graphene oxide	Thermal conductivity	Filler fraction	15–170 mW m^{-1} K^{-1}
Ref. 113	Nanocellulose	Graphene	Specific capacitance	Filler fraction	138–207 F g^{-1}
Ref. 99	Nanocellulose	Graphene	Gauge factor Elongation at break	Filler fraction	7.1–2427 6–100%
Ref. 111	Cellulose	Graphene	Electrical resistance Elongation at break	Filler fraction	1 MΩ–1 kΩ 0.7–3.2%
Ref. 119	Bacterial cellulose	MXene	Capacitance	Filler fraction	550–3400 mF cm^{-2}
Ref. 118	Nanocellulose	MXene	Tensile strength Tensile modulus Electrical conductivity Specific capacitance	Filler fraction	25.8–271.5 MPa 8.25–42 MPa 1–1850 S cm^{-1} 240–348 F g^{-1}
Ref. 126	Nanocellulose	MXene	Tensile strength Tensile modulus	Filler fraction	75.6–136.5 MPa 4.5–9.3 GPa
Ref. 128	Nanocellulose	Hexagonal boron Nntride	Tensile strength	Filler fraction	80–182 MPa
Ref. 120	Nanocellulose	Phosphorene	Optical transparency Power density	Filler fraction	60–90% 0.2–9.36 μW cm^{-2}
Ref. 129	Chitosan	Graphene	Tensile strength Tensile modulus Elongation at break Toughness Electrical conductivity	Filler fraction	100–527 MPa 2.4–19 GPa 1–10% 1.6–17.7 MJ m^{-3} 34.6–155.3 S cm^{-1}
Ref. 131	Chitosan	MXene	Electrical conductivity Effective EMI shielding	Filler fraction	92–1402 S cm^{-1} 26–34.7 dB
Ref. 132	Alginate	Graphene	Tensile strength Tensile modulus Elongation at break Toughness	Filler fraction	75–272 MPa 4.5–9.7 GPa 1.6–7.9% 2–18.1 MJ m^{-3}
Ref. 50	Alginate	MXene	Electrical conductivity Effective EMI shielding	Filler fraction	0.5–4665 S cm^{-1} 15–58 dB
Ref.134	Silk fibroin	Graphene	Tensile strength Tensile modulus Toughness	Filler fraction	75–300 MPa 9.5–145 GPa 0.7–2.4 MJ m^{-3}
Ref. 51	Silk fibroin	MXene	Electrical conductivity	Filler fraction	0.05–1400 S cm^{-1}
Ref. 71	Gelatin	Graphene	Tensile strength Tensile modulus	Filler fraction	10–120 kPa 2–7 kPa
Ref. 140	Gelatin	Graphene	Electrical conductivity	Filler fraction	1 μ–0.1 S cm^{-1}
Ref. 45	Amyloid fibrils	Graphene	Tensile strength Tensile modulus Electrical conductivity	Filler fraction	6–16.5 MPa 2.8–7.2 GPa 50 μ–0.5 S cm^{-1}
Ref. 70	Gelatin	Hexagonal boron nitride	Tensile strength Tensile modulus	Filler fraction	96.4–148.7 MPa 11.8–31 GPa
Ref. 64	Recombinant viral protein	Graphene	Specific capacity	Filler fraction	128–181 mA h g^{-1}
Ref. 142	Recombinant proteins	Graphene	Transconductance	Filler fraction	0.6–1.4 mS
Ref. 10	Recombinant tandem repeat proteins	Graphene	Actuation curvature Actuation power density	Molecular weight (number of repeat units in amino acid sequence)	0.12–1.2 cm^{-1} 0.2–1.2 W cm^{-2}
Ref. 26	Recombinant tandem repeat proteins	MXene	Electrical conductivity	Molecular weight (number of repeat units in amino acid sequence)	30–10 000 S cm^{-1}
Ref. 49	Recombinant tandem repeat proteins	Graphene/ MXene	Tensile strength Elongation at break Toughness	Molecular weight (number of repeat units in amino acid sequence)	100–150 MPa 6–58% 4–55 MJ m^{-3}

interfaces between layers to optimize these properties. The ability to control interfacial chemistry, electrical contact resistance, and thermal boundary resistance using biomolecular interfaces in contact with 2D materials is essential to the flexible 2D devices made from these materials. Additionally, layered 2D systems provide an exciting platform to study the control of optical, electrical, thermal, and mechanical properties in a molecular composite by finely tuning the interlayer distance based on the molecular weight of the biomolecules. By creating programmable 2D materials, we can explore new directions in equilibrium and non-equilibrium materials by studying their phase transition and response to perturbations such as magnetic susceptibility, conductivity, optical reflectivity, and nonlinearity. Moreover, the practical requirements for various functionalities—like achieving waterproof, anti-fouling, conductive, and biocompatible properties—along with intelligent responsiveness, which includes automatically adapting to external factors such as temperature, pH, humidity, and other conditions, are crucial for designing 2D layered materials.

Exploiting the asymmetric transport properties, such as thermal or electrical conductivity, of 2D layered materials requires innovative design rules, which can open up new ways to control emergent physical properties. However, many fundamental challenges still need to be addressed to fully comprehend the capabilities of layered structures in material science and their potential applications in manipulating transport properties. One of the main challenges is the gap between computationally designed and experimentally manufactured materials, which can result in imperfections due to manufacturing and synthesis. To overcome this issue, possible solutions include the directed evolution of biomanufactured materials to enhance robustness or the selection of 2D materials that meet the physical requirements.

In the upcoming years, there will be a notable surge in the exploration of sustainable materials, including a deeper understanding of biomolecules and biodegradable 2D-layered composites. As the production of these materials scales up, biocomposites are expected to become more affordable, accelerating their adoption across various industries, such as automobile, aerospace, and consumer goods. This will not only promote the use of eco-friendly materials but also positively impact the environment.

Author contributions

M. V. and M. C. D. wrote the manuscript. All authors participated in revisions, discussions, and interpretation of the data.

Data availability

No primary research results, software or code have been included and no new data were generated or analysed as part of this review.

Conflicts of interest

The authors declare that the research was conducted without any commercial or financial relationships that could potentially create a conflict of interest.

Acknowledgements

M. V. and M. C. D. were partially supported by DARPA (D19A C00016), Airforce Office of Sponsored Research (FA9550-18-1-0235), Army Research Office (W911NF-16-1-0019), and Huck Endowment of Pennsylvania State University.

References

1 K. S. Novoselov, D. Jiang, F. Schedin, T. J. Booth, V. V. Khotkevich, S. V. Morozov and A. K. Geim, *Proc. Natl. Acad. Sci. U. S. A.*, 2005, **102**, 10451–10453.
2 K. S. Novoselov, A. K. Geim, S. V. Morozov, D. Jiang, Y. Zhang, S. V. Dubonos, I. V. Grigorieva and A. A. Firsov, *Science*, 2004, **306**, 666–670.
3 K. S. Novoselov, A. Mishchenko, A. Carvalho and A. H. Castro Neto, *Science*, 2016, **353**, aac9439.
4 R. J. Young, I. A. Kinloch, L. Gong and K. S. Novoselov, *Compos. Sci. Technol.*, 2012, **72**, 1459–1476.
5 S. Stankovich, D. A. Dikin, G. H. B. Dommett, K. M. Kohlhaas, E. J. Zimney, E. A. Stach, R. D. Piner, S. T. Nguyen and R. S. Ruoff, *Nature*, 2006, **442**, 282–286.
6 M. C. Demirel, M. Vural and M. Terrones, *Adv. Funct. Mater.*, 2018, **28**, 1704990.
7 Z. Ling, C. E. Ren, M.-Q. Zhao, J. Yang, J. M. Giammarco, J. Qiu, M. W. Barsoum and Y. Gogotsi, *Proc. Natl. Acad. Sci. U. S. A.*, 2014, **111**, 16676–16681.
8 Y. Zhang, S. Gong, Q. Zhang, P. Ming, S. Wan, J. Peng, L. Jiang and Q. Cheng, *Chem. Soc. Rev.*, 2016, **45**, 2378–2395.
9 P. Samorì, I. A. Kinloch, X. Feng and V. Palermo, *2D Mater.*, 2015, **2**, 030205.
10 M. Vural, Y. Lei, A. Pena-Francesch, H. Jung, B. Allen, M. Terrones and M. C. Demirel, *Carbon*, 2017, **118**, 404–412.
11 K. W. Putz, O. C. Compton, C. Segar, Z. An, S. T. Nguyen and L. C. Brinson, *ACS Nano*, 2011, **5**, 6601–6609.
12 A. K. Geim and I. V. Grigorieva, *Nature*, 2013, **499**, 419–425.
13 D. Jariwala, T. J. Marks and M. C. Hersam, *Nat. Mater.*, 2016, **16**, 170–181.
14 K. Kalantar-zadeh, J. Z. Ou, T. Daeneke, M. S. Strano, M. Pumera and S. L. Gras, *Adv. Funct. Mater.*, 2015, **25**, 5086–5099.
15 C. Tan and H. Zhang, *Chem. Soc. Rev.*, 2015, **44**, 2713–2731.
16 B. Anasori, M. R. Lukatskaya and Y. Gogotsi, *Nat. Rev. Mater.*, 2017, **2**, 16098.
17 A. VahidMohammadi, J. Rosen and Y. Gogotsi, *Science*, 2021, **372**, eabf1581.
18 M. G. Rasul, A. Kiziltas, B. Arfaei and R. Shahbazian-Yassar, *npj 2D Mater. Appl.*, 2021, **5**, 56.

19 C. R. Dean, A. F. Young, I. Meric, C. Lee, L. Wang, S. Sorgenfrei, K. Watanabe, T. Taniguchi, P. Kim, K. L. Shepard and J. Hone, *Nat. Nanotechnol.*, 2010, **5**, 722–726.
20 D. Lee, S. H. Song, J. Hwang, S. H. Jin, K. H. Park, B. H. Kim, S. H. Hong and S. Jeon, *Small*, 2013, **9**, 2602–2610.
21 H. Mu, S. Lin, Z. Wang, S. Xiao, P. Li, Y. Chen, H. Zhang, H. Bao, S. P. Lau, C. Pan, D. Fan and Q. Bao, *Adv. Opt. Mater.*, 2015, **3**, 1447–1453.
22 G. Hu, T. Albrow-Owen, X. Jin, A. Ali, Y. Hu, R. C. T. Howe, K. Shehzad, Z. Yang, X. Zhu, R. I. Woodward, T.-C. Wu, H. Jussila, J.-B. Wu, P. Peng, P.-H. Tan, Z. Sun, E. J. R. Kelleher, M. Zhang, Y. Xu and T. Hasan, *Nat. Commun.*, 2017, **8**, 278.
23 Z. Zhang, P. Chen, X. Duan, K. Zang, J. Luo and X. Duan, *Science*, 2017, **357**, 788–792.
24 K. S. Kim, D. Lee, C. S. Chang, S. Seo, Y. Hu, S. Cha, H. Kim, J. Shin, J.-H. Lee, S. Lee, J. S. Kim, K. H. Kim, J. M. Suh, Y. Meng, B.-I. Park, J.-H. Lee, H.-S. Park, H. S. Kum, M.-H. Jo, G. Y. Yeom, K. Cho, J.-H. Park, S.-H. Bae and J. Kim, *Nature*, 2023, **614**, 88–94.
25 B.-I. Park, J. Kim, K. Lu, X. Zhang, S. Lee, J. M. Suh, D.-H. Kim, H. Kim and J. Kim, *Nano Lett.*, 2024, **24**, 2939–2952.
26 M. Vural, H. Zhu, A. Pena-Francesch, H. Jung, B. D. Allen and M. C. Demirel, *ACS Nano*, 2020, **14**, 6956–6967.
27 G. Guan, J. Xia, S. Liu, Y. Cheng, S. Bai, S. Y. Tee, Y.-W. Zhang and M.-Y. Han, *Adv. Mater.*, 2017, **29**(32), 1700326.
28 M. Shtein, R. Nadiv, M. Buzaglo, K. Kahil and O. Regev, *Chem. Mater.*, 2015, **27**, 2100–2106.
29 J. Li and J.-K. Kim, *Compos. Sci. Technol.*, 2007, **67**, 2114–2120.
30 I. A. Kinloch, J. Suhr, J. Lou, R. J. Young and P. M. Ajayan, *Science*, 2018, **362**, 547–553.
31 D. Jariwala, V. K. Sangwan, C.-C. Wu, P. L. Prabhumirashi, M. L. Geier, T. J. Marks, L. J. Lauhon and M. C. Hersam, *Proc. Natl. Acad. Sci. U. S. A.*, 2013, **110**, 18076–18080.
32 L. Britnell, R. V. Gorbachev, R. Jalil, B. D. Belle, F. Schedin, A. Mishchenko, T. Georgiou, M. I. Katsnelson, L. Eaves, S. V. Morozov, N. M. R. Peres, J. Leist, A. K. Geim, K. S. Novoselov and L. A. Ponomarenko, *Science*, 2012, **335**, 947–950.
33 T. Georgiou, R. Jalil, B. D. Belle, L. Britnell, R. V. Gorbachev, S. V. Morozov, Y.-J. Kim, A. Gholinia, S. J. Haigh, O. Makarovsky, L. Eaves, L. A. Ponomarenko, A. K. Geim, K. S. Novoselov and A. Mishchenko, *Nat. Nanotechnol.*, 2012, **8**, 100–103.
34 L. Britnell, R. M. Ribeiro, A. Eckmann, R. Jalil, B. D. Belle, A. Mishchenko, Y. Kim, R. V. Gorbachev, T. Georgiou, S. V. Morozov, A. N. Grigorenko, A. K. Geim, C. Casiraghi, A. H. C. Neto and K. S. Novoselov, *Science*, 2013, **340**, 1311–1314.
35 F. Withers, O. Del Pozo-Zamudio, A. Mishchenko, A. P. Rooney, A. Gholinia, K. Watanabe, T. Taniguchi, S. J. Haigh, A. K. Geim, A. I. Tartakovskii and K. S. Novoselov, *Nat. Mater.*, 2015, **14**, 301–306.
36 S. E. Kim, F. Mujid, A. Rai, F. Eriksson, J. Suh, P. Poddar, A. Ray, C. Park, E. Fransson, Y. Zhong, D. A. Muller, P. Erhart, D. G. Cahill and J. Park, *Nature*, 2021, **597**, 660–665.
37 H. Kim, Y. Liu, K. Lu, C. S. Chang, D. Sung, M. Akl, K. Qiao, K. S. Kim, B.-I. Park, M. Zhu, J. M. Suh, J. Kim, J. Jeong, Y. Baek, Y. J. Ji, S. Kang, S. Lee, N. M. Han, C. Kim, C. Choi, X. Zhang, H.-K. Choi, Y. Zhang, H. Wang, L. Kong, N. N. Afeefah, M. N. M. Ansari, J. Park, K. Lee, G. Y. Yeom, S. Kim, J. Hwang, J. Kong, S.-H. Bae, Y. Shi, S. Hong, W. Kong and J. Kim, *Nat. Nanotechnol.*, 2023, **18**, 464–470.
38 S. J. Kim, K. Choi, B. Lee, Y. Kim and B. H. Hong, *Annu. Rev. Mater. Res.*, 2015, **45**, 63–84.
39 H. Jang, Y. J. Park, X. Chen, T. Das, M.-S. Kim and J.-H. Ahn, *Adv. Mater.*, 2016, **28**, 4184–4202.
40 M. Vural, A. Pena-Francesch, J. Bars-Pomes, H. Jung, H. Gudapati, C. B. Hatter, B. Allen, B. Anasori, I. T. Ozbolat, Y. Gogotsi and M. C. Demirel, *Adv. Funct. Mater.*, 2018, **28**, 1801972.
41 X. Zhang, L. Hou, A. Ciesielski and P. Samorì, *Adv. Energy Mater.*, 2016, **6**, 1600671.
42 F. Bonaccorso, L. Colombo, G. Yu, M. Stoller, V. Tozzini, C. Ferrari, R. S. Ruoff and V. Pellegrini, *Science*, 2015, **347**, 1246501.
43 Q. Xue, H. Zhang, M. Zhu, Z. Pei, H. Li, Z. Wang, Y. Huang, Y. Huang, Q. Deng, J. Zhou, S. Du, Q. Huang and C. Zhi, *Adv. Mater.*, 2017, **29**, 1604847.
44 J. Kuchlyan, N. Kundu, D. Banik, A. Roy and N. Sarkar, *Langmuir*, 2015, **31**, 13793–13801.
45 C. Li, J. Adamcik and R. Mezzenga, *Nat. Nanotechnol.*, 2012, **7**, 421–427.
46 J. Lee, P. Dak, Y. Lee, H. Park, W. Choi, M. A. Alam and S. Kim, *Sci. Rep.*, 2015, **4**, 7352.
47 L. Wang, Y. Wang, J. I. Wong, T. Palacios, J. Kong and H. Y. Yang, *Small*, 2014, **10**, 1101–1105.
48 K. Kalantar-zadeh and J. Z. Ou, *ACS Sens.*, 2016, **1**, 5–16.
49 M. Vural, T. Mazeed, D. Li, O. Colak, R. F. Hamilton, H. Gao and M. C. Demirel, *Proc. Natl. Acad. Sci. U. S. A.*, 2022, **119**(31), e2120021119.
50 F. Shahzad, M. Alhabeb, C. B. Hatter, B. Anasori, S. Man Hong, C. M. Koo and Y. Gogotsi, *Science*, 2016, **353**, 1137–1140.
51 M. C. Krecker, D. Bukharina, C. B. Hatter, Y. Gogotsi and V. V. Tsukruk, *Adv. Funct. Mater.*, 2020, **30**, 2004554.
52 G. Guan, S. Zhang, S. Liu, Y. Cai, M. Low, C. P. Teng, I. Y. Phang, Y. Cheng, K. L. Duei, B. M. Srinivasan, Y. Zheng, Y. W. Zhang and M. Y. Han, *J. Am. Chem. Soc.*, 2015, **137**, 6152–6155.
53 L. Zong, M. Li and C. Li, *Adv. Mater.*, 2017, **29**, 1604691.
54 H. B. Sim, J. Y. Lee, B. Park, S. J. Kim, S. Kang, W. H. Ryu and S. C. Jun, *Nano Res.*, 2016, **9**, 1709–1722.
55 D. Akinwande, C. J. Brennan, J. S. Bunch, P. Egberts, J. R. Felts, H. Gao, R. Huang, J.-S. Kim, T. Li, Y. Li, K. M. Liechti, N. Lu, H. S. Park, E. J. Reed, P. Wang, B. I. Yakobson, T. Zhang, Y.-W. Zhang, Y. Zhou and Y. Zhu, *Extreme Mech. Lett.*, 2017, **13**, 42–77.

56 Y. Cheng, L. D. Koh, D. Li, B. Ji, Y. Y. W. Zhang, J. Yeo, G. Guan, M. Y. Han and Y. Y. W. Zhang, *ACS Appl. Mater. Interfaces*, 2015, **7**, 21787–21796.
57 A. Moudgil, N. Kalyani, G. Sinsinbar, S. Das and P. Mishra, *ACS Appl. Mater. Interfaces*, 2018, **10**, 4866–4873.
58 N. Song, D. Jiao, S. Cui, X. Hou, P. Ding and L. Shi, *ACS Appl. Mater. Interfaces*, 2017, **9**, 2924–2932.
59 G. Song, R. Kang, L. Guo, Z. Ali, X. Chen, Z. Zhang, C. Yan, C.-T. Lin, N. Jiang and J. Yu, *New J. Chem.*, 2020, **44**, 7186–7193.
60 W. Yang, Z. Zhao, K. Wu, R. Huang, T. Liu, H. Jiang, F. Chen and Q. Fu, *J. Mater. Chem. C*, 2017, **5**, 3748–3756.
61 W.-T. Cao, F.-F. Chen, Y.-J. Zhu, Y.-G. Zhang, Y.-Y. Jiang, M.-G. Ma and F. Chen, *ACS Nano*, 2018, **12**, 4583–4593.
62 B. Liang, L. Fang, Y. Hu, G. Yang, Q. Zhu and X. Ye, *Nanoscale*, 2014, **6**, 4264–4274.
63 M. Qi, Y. Zhou, Y. Huang, L. Zhu, X. Xu, Z. Ren and J. Bai, *Nanoscale*, 2017, 637–646.
64 D. Oh, X. Dang, H. Yi, M. A. Allen, K. Xu, Y. J. Lee and A. M. Belcher, *Small*, 2012, **8**, 1006–1011.
65 S. Wan, J. Peng, L. Jiang and Q. Cheng, *Adv. Mater.*, 2016, **28**, 7862–7898.
66 T. Benselfelt, J. Shakya, P. Rothemund, S. B. Lindström, A. Piper, T. E. Winkler, A. Hajian, L. Wågberg, C. Keplinger and M. M. Hamedi, *Adv. Mater.*, 2023, **35**, 2303255.
67 N. Annabi, S. R. Shin, A. Tamayol, M. Miscuglio, M. A. Bakooshli, A. Assmann, P. Mostafalu, J. Y. Sun, S. Mithieux, L. Cheung, X. Tang, A. S. Weiss and A. Khademhosseini, *Adv. Mater.*, 2016, **28**, 40–49.
68 S.-H. H. Hu, R.-H. H. Fang, Y.-W. W. Chen, B.-J. J. Liao, I.-W. W. Chen and S.-Y. Y. Chen, *Adv. Funct. Mater.*, 2014, **24**, 4144–4155.
69 R. Deng, H. Yi, F. Fan, L. Fu, Y. Zeng, Y. Wang, Y. Li, Y. Liu, S. Ji and Y. Su, *RSC Adv.*, 2016, **6**, 77083–77092.
70 S. C. Yoo, Y. K. Park, C. Park, H. Ryu and S. H. Hong, *Adv. Funct. Mater.*, 2018, **28**, 1805948.
71 C. Cha, S. R. Shin, X. Gao, N. Annabi, M. R. Dokmeci, X. (Shirley) Tang and A. Khademhosseini, *Small*, 2014, **10**, 514–523.
72 C. Ye, Z. A. Combs, R. Calabrese, H. Dai, D. L. Kaplan and V. V. Tsukruk, *Small*, 2014, **10**, 5087–5097.
73 E. A. Mayerberger, R. M. Street, R. M. McDaniel, M. W. Barsoum and C. L. Schauer, *RSC Adv.*, 2018, **8**, 35386–35394.
74 W. Yin, L. Yan, J. Yu, G. Tian, L. Zhou, X. Zheng, X. Zhang, Y. Yong, J. Li, Z. Gu and Y. Zhao, *ACS Nano*, 2014, **8**, 6922–6933.
75 H. Bao, Y. Pan, Y. Ping, N. G. Sahoo, T. Wu, L. Li, J. Li and L. H. Gan, *Small*, 2011, **7**, 1569–1578.
76 C. Li, Z.-Y. Wu, H.-W. Liang, J.-F. Chen and S.-H. Yu, *Small*, 2017, **13**, 1700453.
77 C. Zhu, P. Liu and A. P. Mathew, *ACS Appl. Mater. Interfaces*, 2017, **9**, 21048–21058.
78 C. Zhu, S. Monti and A. P. Mathew, *ACS Nano*, 2018, **12**, 7028–7038.
79 M. Abolhassani, C. S. Griggs, L. A. Gurtowski, J. A. Mattei-Sosa, M. Nevins, V. F. Medina, T. A. Morgan and L. F. Greenlee, *ACS Omega*, 2017, **2**, 8751–8759.
80 Y. Wang, A. G. El-Deen, P. Li, B. H. L. Oh, Z. Guo, M. M. Khin, Y. S. Vikhe, J. Wang, R. G. Hu, R. M. Boom, K. A. Kline, D. L. Becker, H. Duan and M. B. Chan-Park, *ACS Nano*, 2015, **9**(10), 10142–10157.
81 A. K. K. Geim and K. S. S. Novoselov, *Nat. Mater.*, 2007, **6**, 183–191.
82 D. A. Dikin, S. Stankovich, E. J. Zimney, R. D. Piner, G. H. Dommett, G. Evmenenko, S. T. Nguyen and R. S. Ruoff, *Nature*, 2007, **448**, 457–460.
83 Y. Fu, J. Hansson, Y. Liu, S. Chen, A. Zehri, M. K. Samani, N. Wang, Y. Ni, Y. Zhang, Z.-B. Zhang, Q. Wang, M. Li, H. Lu, M. Sledzinska, C. M. S. Torres, S. Volz, A. A. Balandin, X. Xu and J. Liu, *2D Mater.*, 2019, **7**, 12001.
84 H. Jang, J. D. Wood, C. R. Ryder, M. C. Hersam and D. G. Cahill, *Adv. Mater.*, 2015, **27**, 8017–8022.
85 S. B. Jo, H. H. Kim, H. Lee, B. Kang, S. Lee, M. Sim, M. Kim, W. H. Lee and K. Cho, *ACS Nano*, 2015, **9**, 8206–8219.
86 G. Cassabois, P. Valvin and B. Gil, *Nat. Photonics*, 2015, **10**, 262–266.
87 J. Simon, C. Fruhling, H. Kim, Y. Gogotsi and A. Boltasseva, *Opt. Photonics News*, 2023, **34**, 42–49.
88 C. R. So, Y. Hayamizu, H. Yazici, C. Gresswell, D. Khatayevich, C. Tamerler and M. Sarikaya, *ACS Nano*, 2012, **6**, 1648–1656.
89 A. J. Patil, J. L. Vickery, T. B. Scott and S. Mann, *Adv. Mater.*, 2009, **21**, 3159–3164.
90 H. Zhu, Z. Jia, Y. Chen, N. Weadock, J. Wan, O. Vaaland, X. Han, T. Li and L. Hu, *Nano Lett.*, 2013, **13**, 3093–3100.
91 A. Pena-Francesch, H. Jung, M. C. Demirel and M. Sitti, *Nat. Mater.*, 2020, **19**, 1230–1235.
92 A. Pena-Francesch, H. Jung, M. C. Demirel and M. Sitti, *Nat. Mater.*, 2020, **19**, 1230–1235.
93 H. Zhu, Y. Li, Z. Fang, J. Xu, F. Cao, J. Wan, C. Preston, B. Yang and L. Hu, *ACS Nano*, 2014, **8**, 3606–3613.
94 K. Wu, J. Fang, J. Ma, R. Huang, S. Chai, F. Chen and Q. Fu, *ACS Appl. Mater. Interfaces*, 2017, **9**, 30035–30045.
95 V. Nicolosi, M. Chhowalla, M. G. Kanatzidis, M. S. Strano and J. N. Coleman, *Science*, 2013, **340**, 1226419.
96 J. N. Coleman, M. Lotya, A. O'Neill, S. D. Bergin, P. J. King, U. Khan, K. Young, A. Gaucher, S. De, R. J. Smith, I. V. Shvets, S. K. Arora, G. Stanton, H.-Y. Kim, K. Lee, G. T. Kim, G. S. Duesberg, T. Hallam, J. J. Boland, J. J. Wang, J. F. Donegan, J. C. Grunlan, G. Moriarty, A. Shmeliov, R. J. Nicholls, J. M. Perkins, E. M. Grieveson, K. Theuwissen, D. W. McComb, P. D. Nellist and V. Nicolosi, *Science*, 2011, **331**, 568–571.
97 P. Laaksonen, M. Kainlauri, T. Laaksonen, A. Shchepetov, H. Jiang, J. Ahopelto and M. B. Linder, *Angew. Chem., Int. Ed.*, 2010, **49**, 4946–4949.
98 N. I. Kovtyukhova, Y. Wang, A. Berkdemir, R. Cruz-Silva, M. Terrones, V. H. Crespi and T. E. Mallouk, *Nat. Chem.*, 2014, **6**, 957–963.
99 C. Yan, J. Wang, W. Kang, M. Cui, X. Wang, C. Y. Foo, K. J. Chee and P. S. Lee, *Adv. Mater.*, 2014, **26**, 2022–2027.
100 U. G. K. Wegst, H. Bai, E. Saiz, A. P. Tomsia and R. O. Ritchie, *Nat. Mater.*, 2015, **14**, 23–36.

101 H. Zhu, W. Luo, P. N. Ciesielski, Z. Fang, J. Y. Zhu, G. Henriksson, M. E. Himmel and L. Hu, *Chem. Rev.*, 2016, **116**, 9305–9374.
102 A. Pena-Francesch, N. E. Domeradzka, H. Jung, B. Barbu, M. Vural, Y. Kikuchi, B. D. Allen and M. C. Demirel, *APL Mater.*, 2018, **6**, 10701.
103 J.-M. Malho, P. Laaksonen, A. Walther, O. Ikkala and M. B. Linder, *Biomacromolecules*, 2012, **13**, 1093–1099.
104 N. Song, X. Hou, L. Chen, S. Cui, L. Shi and P. Ding, *ACS Appl. Mater. Interfaces*, 2017, **9**, 17914–17922.
105 B. Wicklein, A. Kocjan, G. Salazar-Alvarez, F. Carosio, G. Camino, M. Antonietti and L. Bergström, *Nat. Nanotechnol.*, 2015, **10**, 277–283.
106 J. Chen, X. Huang, Y. Zhu and P. Jiang, *Adv. Funct. Mater.*, 2017, **27**, 1604754.
107 S.-S. Kim, J.-H. Jeon, H.-I. Kim, C. D. Kee and I.-K. Oh, *Adv. Funct. Mater.*, 2015, **25**, 3560–3570.
108 Y. Li, H. Zhu, F. Shen, J. Wan, X. Han, J. Dai, H. Dai and L. Hu, *Adv. Funct. Mater.*, 2014, **24**, 7366–7372.
109 Z. Zhou, J. Liu, X. Zhang, D. Tian, Z. Zhan and C. Lu, *Adv. Mater. Interfaces*, 2019, **6**, 1802040.
110 A. C. E. Camilo, A. J. de Menezes, M. A. Pereira-da-Silva, F. E. G. Guimarães and R. H. Longaresi, *Cellulose*, 2020, **27**, 713–728.
111 Z. Weng, Y. Su, D.-W. Wang, F. Li, J. Du and H.-M. Cheng, *Adv. Energy Mater.*, 2011, **1**, 917–922.
112 L. Liu, Z. Niu, L. Zhang, W. Zhou, X. Chen and S. Xie, *Adv. Mater.*, 2014, **26**, 4855–4862.
113 K. Gao, Z. Shao, J. Li, X. Wang, X. Peng, W. Wang and F. Wang, *J. Mater. Chem. C*, 2013, **1**, 63–67.
114 Y. Habibi, L. A. Lucia and O. J. Rojas, *Chem. Rev.*, 2010, **110**, 3479–3500.
115 W. S. Lee and J. Choi, *ACS Appl. Mater. Interfaces*, 2019, **11**, 19363–19371.
116 C. Yoo, M. G. Kaium, L. Hurtado, H. Li, S. Rassay, J. Ma, T.-J. Ko, S. S. Han, M. S. Shawkat, K. H. Oh, H.-S. Chung and Y. Jung, *ACS Appl. Mater. Interfaces*, 2020, **12**, 25200–25210.
117 F. Lai, D. Yong, X. Ning, B. Pan, Y.-E. Miao and T. Liu, *Small*, 2017, **13**, 1602866.
118 W. Tian, A. VahidMohammadi, M. S. Reid, Z. Wang, L. Ouyang, J. Erlandsson, T. Pettersson, L. Wågberg, M. Beidaghi and M. M. Hamedi, *Adv. Mater.*, 2019, **31**, 1902977.
119 Y. Wang, X. Wang, X. Li, Y. Bai, H. Xiao, Y. Liu, R. Liu and G. Yuan, *Adv. Funct. Mater.*, 2019, **29**, 1900326.
120 P. Cui, K. Parida, M.-F. Lin, J. Xiong, G. Cai and P. S. Lee, *Adv. Mater. Interfaces*, 2017, **4**, 1700651.
121 R. Xiong, K. Hu, A. M. Grant, R. Ma, W. Xu, C. Lu, X. Zhang and V. V. Tsukruk, *Adv. Mater.*, 2016, **28**, 1501–1509.
122 Y. Liu, J. Zhou, E. Zhu, J. Tang, X. Liu and W. Tang, *J. Mater. Chem. C*, 2015, **3**, 1011–1017.
123 Y. Liu, J. Zhou, J. Tang and W. Tang, *Chem. Mater.*, 2015, **27**, 7034–7041.
124 P. Laaksonen, A. Walther, J. M. Malho, M. Kainlauri, O. Ikkala and M. B. Linder, *Angew. Chem., Int. Ed.*, 2011, **50**, 8688–8691.
125 N. D. Luong, N. Pahimanolis, U. Hippi, J. T. Korhonen, J. Ruokolainen, L.-S. Johansson, J.-D. Nam and J. Seppälä, *J. Mater. Chem.*, 2011, **21**, 13991–13998.
126 W.-T. Cao, C. Ma, D.-S. Mao, J. Zhang, M.-G. Ma and F. Chen, *Adv. Funct. Mater.*, 2019, **29**, 1905898.
127 W. Tian, A. VahidMohammadi, M. S. Reid, Z. Wang, L. Ouyang, J. Erlandsson, T. Pettersson, L. Wågberg, M. Beidaghi and M. M. Hamedi, *Adv. Mater.*, 2019, **31**, 1902977.
128 Y. Li, H. Zhu, F. Shen, J. Wan, S. Lacey, Z. Fang, H. Dai and L. Hu, *Nano Energy*, 2015, **13**, 346–354.
129 S. Wan, J. Peng, Y. Li, H. Hu, L. Jiang and Q. Cheng, *ACS Nano*, 2015, **9**, 9830–9836.
130 M. Naguib, *ACS Cent. Sci.*, 2020, **6**, 344–346.
131 F. Liu, Y. Li, S. Hao, Y. Cheng, Y. Zhan, C. Zhang, Y. Meng, Q. Xie and H. Xia, *Carbohydr. Polym.*, 2020, **243**, 116467.
132 K. Chen, B. Shi, Y. Yue, J. Qi and L. Guo, *ACS Nano*, 2015, **9**, 8165–8175.
133 S. Wan, J. Peng, Y. Li, H. Hu, L. Jiang and Q. Cheng, *ACS Nano*, 2015, **9**, 9830–9836.
134 K. Hu, M. K. Gupta, D. D. Kulkarni and V. V. Tsukruk, *Adv. Mater.*, 2013, **25**, 2301–2307.
135 A. P. Liu, E. A. Appel, P. D. Ashby, B. M. Baker, E. Franco, L. Gu, K. Haynes, N. S. Joshi, A. M. Kloxin, P. H. J. Kouwer, J. Mittal, L. Morsut, V. Noireaux, S. Parekh, R. Schulman, S. K. Y. Tang, M. T. Valentine, S. L. Vega, W. Weber, N. Stephanopoulos and O. Chaudhuri, *Nat. Mater.*, 2022, **21**, 390–397.
136 M. Ding, D. Ji and W. Hu, *ACS Appl. Electron. Mater.*, 2024, **6**(12), 8655–8670.
137 S. Yang, Y. Zhu, J. Liu, X. Zheng, X. Zhang and P. Liu, *Int. J. Hydrogen Energy*, 2023, **48**(49), 18708–18718.
138 K. W. Liu, Y. B. Ma, Y. Guo, H. Wang, Y. N. Xu, X. D. Zhang, X. Zhang, X. Z. Sun, K. Wang, L. Yu and Y. W. Ma, *Adv. Funct. Mater.*, 2024, **34**, 2410451.
139 J. Liu, S. Fu, B. Yuan, Y. Li and Z. Deng, *J. Am. Chem. Soc.*, 2010, **132**, 7279–7281.
140 H. Nassira, A. Sánchez-Ferrer, J. Adamcik, S. Handschin, H. Mahdavi, N. Taheri Qazvini and R. Mezzenga, *Adv. Mater.*, 2016, 6914–6920.
141 L. Liu, Z. Liu, P. Huang, Z. Wu and S. Jiang, *RSC Adv.*, 2016, **6**, 113315.
142 Y. Hayamizu, C. R. So, S. Dag, T. S. Page, D. Starkebaum and M. Sarikaya, *Sci. Rep.*, 2016, **6**, 33778.
143 E. Wang, M. S. Desai, K. Heo and S. W. Lee, *Langmuir*, 2014, **30**, 2223–2229.
144 E. Wang, M. S. Desai and S. W. Lee, *Nano Lett.*, 2013, **13**, 2826–2830.
145 T. H. Han, W. J. Lee, D. H. Lee, J. E. Kim, E. Y. Choi and S. O. Kim, *Adv. Mater.*, 2010, **22**, 2060–2064.
146 Z. Wang, S. Kang, S. Cao, M. Krecker, V. V. Tsukruk and S. Singamaneni, *MRS Bull.*, 2020, **45**, 1017–1026.
147 F. Meng, B. Sana, Y. Li, Y. Liu, S. Lim and X. Chen, *Small*, 2014, **10**, 277–283.
148 H. Wang, B. Zhu, H. Wang, X. Ma, Y. Hao and X. Chen, *Small*, 2016, **12**, 3360–3365.

149 M. Wang, S. Zhang, Z. Ye, L. He, F. Yan, Y. Yang, H. Zhang and Z. Zhang, *Microchim. Acta*, 2015, **182**, 2251–2258.
150 X. He, H. Han, W. Shi, J. Dong, X. Lu, W. Yanga and X. Lu, *Anal. Methods*, 2020, **12**, 3462–3469.
151 H. Jung, A. Pena-Francesch, A. Saadat, A. Sebastian, D. H. Kim, R. F. Hamilton, I. Albert, B. D. Allen and M. C. Demirel, *Proc. Natl. Acad. Sci. U. S. A.*, 2016, **113**, 6478–6483.